Antibody-mediated SARS-CoV-2 entry and conformational regulation

Casey L. Kiyohara

A dissertation

submitted in partial fulfillment of the

requirements for the degree of

Doctor of Philosophy

University of Washington

2023

Reading Committee:

Wendy E. Thomas, Chair

Michael Regnier

Susan Fink

Program Authorized to Offer Degree:

Bioengineering

University of Washington

Abstract

Antibody-mediated SARS-CoV-2 entry and conformational regulation

Casey L. Kiyohara

Chair of the Supervisory Committee:

Wendy Thomas

Department of Bioengineering

Antibody-mediated entry (AME) of SARS-CoV-2 into monocytes and macrophages has been linked to activation of inflammatory phenotypes that are associated with severe COVID-19[1], but why only some antibodies mediate this entry while others do not is unknown. However, it has been demonstrated that conformational dynamics of the SARS-CoV-2 receptor binding domain (RBD) are critical to viral entry [2–7], and that antibodies targeting the RBD can conformationally regulate these dynamics[5–9]. Here, we identified 5 groups of mAbs that target unique epitopes on the SARS-CoV-2 RBD and also are associated with different RBD conformational regulation and AME abilities. Structure alignment and antibody docking analysis elucidated a thermodynamic basis for differences in conformational regulation by these antibody groups. We

found that some, but not all, antibody groups were able to mediate entry into THP1-derived macrophages, and also found that this entry was inhibitable by mAbs in other groups. Collectively, these results suggest that there is a connection between RBD conformational regulation, epitope, and AME ability of antibodies. This connection improves understanding of the AME mechanism and how to inhibit AME for SARS-CoV-2, which has potential applications in the continued development of safe and effective vaccines and therapeutics for COVID-19 and related diseases.

Table of Contents

List of Figures

List of Tables

Acknowledgements

I am endlessly grateful for the countless people who have played a significant role in supporting me professionally, scientifically, and personally over the last six years and for many, many years before that.

To my parents, thank you for giving me the personal and academic foundation to be able to pursue my Ph.D. I am so grateful for the daily support and encouragement you provided me with through the many ups and downs of graduate school, and for the same support that you have given me throughout my whole life. I would not be where I am without it, or you.

To my advisor, Wendy Thomas, thank you for being an incredible mentor to me both inside and outside the research lab. You have given me such incredibly well-rounded support over the past six years that I am leaving your lab as not only a better scientist, but also a better mentor, advocate (for myself and others), writer, leader, and person.

To my Supervisory Committee, Michael Regnier, Evgeni Sokurenko, Linda Wordeman, and Susan Fink, thank you for your feedback, time, and expertise over the years. I have grown and learned so much under your mentorship. Mike, thank you for also being so supportive of me as your rotation student, your teaching assistant, and your BCTP trainee. I am grateful to have had many opportunities to continue interfacing with you throughout my Ph.D.

To my collaborators in the Polyak, Fink, Bloom, and Gale Labs, particularly Stephen Polyak, Jessica Wagoner, Andreas B. Den Hartigh Katharine Crawford, Keara Malone, and Andrey Shuvarikov, thank you for the many, many Zoom meetings and time spent training and troubleshooting with me. Your generosity and expertise made this project possible.

To my colleagues in the Thomas/Interlandi Labs over the years, in particular Molly Mollica, Laura Carlucci, Eric Pederson, Lesley Martínez Rodríguez, Amy Stegmann, Olga Filippova, An-Yue Tu, and Gianluca Interlandi, thank you for all of the feedback and advice on my experiments, data, and practice presentations, the adventures at and outside of work, and the reminders that “it will be fine!!” You made it so much more fun to come to work every day.

To my Thomas Lab undergraduate mentees, Varun Kamat, Lucy Liu, and Sheamin Kim, thank you for your enthusiasm, dedication, time, and patience. Lucy, you did incredible work helping get this project off the ground, and I am excited to watch you continue to pursue and excel at your goals. Sheamin, I know that I have asked an incredible amount of you over the past year. I am so grateful for and impressed by the way you have taken it all in stride, become my co-expert on all the assays used in this work, and grown so much so quickly as a scientist.

To the many teachers and mentors I have had throughout my life who instilled in me my love for science and learning and showed me how far I could go, thank you for your contagious enthusiasm – I have never stopped chasing it.

To my friends, both from UW and from home, and my family, both old and new, thank you for being both the life and the balance in my work-life balance. I have gained so much during my time in Seattle, and the laughs, adventures, and memories with you have been the best of it all.

To Molly, thank you for being on my team in all the ways I do and don’t see, for reminding me to be silly, and for believing in me every single day. I’m having the time of my life fighting dragons with you.

Chapter I: Introduction

Coronavirus disease 2019 (COVID-19) is caused by infection with severe acute respiratory syndrome coronavirus 2 (SARS-CoV-2)[10]. Entry of SARS-CoV-2 into host cells expressing angiotensin-converting enzyme 2 (ACE2) is mediated by conformational dynamics of the receptor binding domain (RBD) on the SARS-CoV-2 spike protein[4,11,12]. In addition to SARS-CoV-2 infection of ACE2-expressing cells, COVID-19 patients show infection of ACE2-negative macrophages and monocytes, which subsequently develop an inflammatory phenotype that may contribute to cytokine storms associated with severe disease[13–15]. It has been demonstrated that *in vitro*, some antibodies targeting the SARS-CoV-2 spike RBD can allow the virus to bind and enter cells via Fcγ receptors (FcγRs)[1,16,17], but why some antibodies mediate entry and infection and others do not is not fully understood. Given the key role of SARS-CoV-2 RBD dynamics in viral binding and fusion[12], and the ability of antibodies to control these dynamics[5–8,18], we hypothesize that conformational regulation of these RBD dynamics by antibodies has a key role in antibody ability to mediate FcγR-dependent AME.

Prior to viral binding, the SARS-CoV-2 RBD is known to switch between an “up” conformation exposing the ACE2 binding site and a “down” conformation in which the site is masked[12]. We therefore hypothesize that certain antibody epitopes, and the accessibility of these epitopes in the up and down RBD conformations are associated with differences in antibody ability to affect this conformational regulation and mediate entry of virus into FcγR-expressing cells. Chapter III of this work, “Epitope and structure basis for antibody differences in SARS-CoV-2 conformational regulation and antibody-mediated entry,” uses analysis of previously published antibody structures to investigate this hypothesis.

SARS-CoV-2 neutralizing antibodies have varying abilities to conformationally regulate the SARS-CoV-2 RBD. We hypothesize that this conformational regulation is associated with differences in AME into FcγR-expressing cells. Chapter IV of this work, “Neutralization and antibody-mediated entry ability for anti-SARS-CoV-2 antibodies of different groups,” uses experimental approaches to investigate this hypothesis.

Better understanding of RBD conformational regulation in SARS-CoV-2 AME supports efforts to identify and inhibit AME, which have implications in the continued development of safe and effective vaccines and therapeutics for COVID-19. We hypothesize that neutralizing antibodies with varying RBD conformational regulation will also inhibit AME. Chapter V of this work, “Antibody inhibition of SARS-CoV-2 AME,” seeks to compare competitive and conformational mechanisms to inhibit AME into FcγR-expressing cells.

Collectively, these aims will investigate the relationship between SARS-CoV-2 RBD conformational regulation, epitope, and AME ability into FcγR-expressing cells for monoclonal antibodies. Understanding these factors that may affect AME will help improve understanding of the AME mechanism and could drive future development of AME inhibitors and non-AME-inducing therapeutics and vaccines. This approach could improve treatment and care for COVID-19 and diseases caused by related viruses and mechanisms.

Chapter II: Background

2.1 COVID-19 pandemic and disease

Despite the rapid development and administration of vaccines to protect against coronavirus disease 2019 (COVID-19), the pandemic continues to persist globally. Continued spread of COVID-19 is driven in part by the emergence of highly transmissible and immune-evasive variants of severe acute respiratory syndrome coronavirus 2 (SARS-CoV-2), the virus that causes COVID-19[10].

Severe COVID-19 often presents with a macrophage activation syndrome (MAS)-type phenotype, which is characterized by the release of high levels of inflammatory cytokines, including IL-1, IL-6, TNF-α, G-CSF, and CXCL10, by immune cells[13,14]. In COVID-19, this hyperinflammatory "cytokine storm" is particularly localized to lung tissues, with activation of immune cells such as alveolar macrophages resident in the lungs[13,14]. This localized cytokine storm can activate inflammatory pathways and recruit additional immune cells to the site of infection, leading to effects such as pulmonary intravascular coagulopathy and acute respiratory distress syndrome (ARDS) with limited systemic macrophage activation and cytokine release[13,14].

2.2 SARS-CoV-2 cell entry

SARS-CoV-2 is a positive-sense, single-stranded RNA virus[12]. Similarly to SARS-CoV, it initiates cell infection by binding to angiotensin-converting enzyme 2 (ACE2) on host cells via its spike protein[4,11]. The SARS-CoV-2 spike protein is a homotrimer, with each protomer consisting of a receptor-binding-domain (RBD)-containing S1 subunit and a membrane-anchored and fusion-mediating S2 subunit[4,11,12]. During viral synthesis, the SARS-CoV-2 spike protein undergoes a priming cleavage at the S1/S2 interface by proprotein convertases such as furin[4,19]. Binding of the

S1 subunit to ACE2 exposes a second cleavage site, S2', which is cleaved by transmembrane protease, serine 2 (TMPRSS2) at the plasma membrane of epithelial cells or cathepsin L at the endosomal membrane, for TMPRSS2-negative cells[12,19]. Following S2' cleavage, the spike S1 subunit is released, or shed, from the S2 subunit, which subsequently undergoes significant conformational changes into its postfusion conformation[12]. During this conformational change to the postfusion conformation, an intermediate spike state exposes the fusion peptide in the S2 subunit, initiating fusion of the viral and cell membranes that allows the viral genome to enter the cell cytoplasm[12].

2.3 FcγR-dependent antibody-mediated entry (AME) in SARS-CoV-2

2.3.1 Clinical relevance of SARS-CoV-2 AME into ACE2-negative FcγR-expressing cells

Several viruses such as Dengue, HIV, and Ebola have demonstrated antibody-dependent enhancement (ADE) of viral infection, where subneutralizing levels of antibodies targeting the virus facilitate entry into and production of live virus inside FcγR-expressing cells by allowing binding to FcγRs[20]. For the Dengue virus, ADE can occur upon reinfection with a different strain of the virus that is not neutralized by antibodies developed during the initial infection, and ADE in FcγR-expressing cells leads to more severe disease for the second infection[20]. In contrast to these viruses, it has been shown that while SARS-CoV-2 can undergo antibody-mediated entry (AME) into FcγR-expressing cells[1,15–17,21], this infection is abortive, not leading to replication of live virus inside the cell[15,22].

However, there is evidence that infection of FcγR-expressing cells, particularly monocytes and macrophages, is relevant to COVID-19 disease despite being abortive. One recent study found that ~10% of blood monocytes and ~8% of tissue-resident lung macrophages isolated from

COVID-19 patients are infected with SARS-CoV-2, despite both cell types lacking ACE2 expression[15]. These infected cells also showed activation of inflammasomes, cause release of IL-1 cytokines and initiation of pyroptosis, an inflammatory form of cell death that leads to further cytokine release and immune cell recruitment[15]. Key markers of pyroptosis, including IL-1RA and IL-18 were elevated in COVID-19 patient blood compared to that of healthy donors[15]. Notably, these pyroptosis markers were particularly elevated for severe COVID-19 patients relative to patients with mild or moderate disease[15]. In addition, monocytopenia, or depletion of monocytes, has been associated with severe COVID-19 [23], with programmed cell death being a hypothesized cause[24], further supporting clinical relevance of this pyroptosis. Similarly, lymphocytes express FcγRs associated with SARS-CoV-2 AME[16,25]. Lymphocytopenia has been shown in COVID-19 patients with severe disease, which may be related to their decreased ability to target and eliminate infected cells, such as monocytes, to control infection and inflammation within these cells[23]. Collectively, these results suggest that FcγR-dependent infection of FcγR-expressing cells, particularly monocytes and macrophages, causes inflammatory cell death and cytokine release that affects COVID-19 disease.

This recent study supports previous results showing SARS-CoV-2 infection of ACE2-negative monocyte-derived and tissue-resident macrophages isolated from COVID-19 patient lungs[26–28], although, notably, one study found that tissue-resident macrophages do express ACE2[29]. In addition, several studies have found that monocytes and macrophages isolated from COVID-19 patients have higher expression of inflammatory cytokines and chemokines[26–28]. Given the key role of cytokine storms localized in the lungs in COVID-19 disease[14], these studies demonstrating SARS-CoV-2 infection and subsequent inflammation and cytokine release by ACE2-negative

macrophages and monocytes isolated from COVID-19 patients support the clinical relevance of AME even without productive internal viral replication.

2.3.2 AME mechanism

It has been shown that AME via FcγRIIb is inhibited by inhibitors of macropinocytosis, endocytosis, phoinositide 5-kinase activity, and lysosome acidification[16]. Notably, low pH is required for cleavage of the spike by endosomal and lysosomal proteases and subsequent viral fusion with host cell[30]. Therefore, AME likely requires not only viral binding to FcγRs, but also endocytosis of the antibody-viral complex, followed by spike cleavage and viral fusion[16]. An additional study also found that EK1, a peptide that prevents viral fusion, inhibited AME, but importantly, this work has yet to be officially peer-reviewed and published[21].

Although AME of SARS-CoV-2 into FcγR-expressing cells has been demonstrated for both mAbs[1,16,17] and COVID-19 patient serum[31,32], why some mAbs and serum mediate entry and others do not is not fully understood. All mAbs capable of causing AME that have been published have to our knowledge been shown to mediate entry at an intermediate concentration of antibody, with low and high concentrations of antibody losing the effect[1,16,17]. Similarly, one study on COVID-19 patient serum saw the most SARS-CoV-2 AME of FcγRIIb-expressing Raji cells at an intermediate serum dilution[31]. Additionally, SARS-CoV-2 AME mAbs have to our knowledge all been shown to neutralize entry into ACE2-expressing cells[1,16,17] and most, but not all[17], bind the SARS-CoV-2 RBD[1,16]. One paper identified four main epitope groups through competition assays and found that one group was associated with AME into Raji cells[17].

Wang et al.[16] found that both of the AME antibodies their study identified required a bivalent interaction with the SARS-CoV-2-spike to mediate entry into FcγR-expressing cells, suggesting

potential cross-linking between spike protomers or trimers. It has also been demonstrated that more highly afucosylated antibodies led to more AME of healthy donor monocytes than less afucosylated antibodies[15]. Afucosylated antibodies have 10- to 100-fold higher affinity for FcγRIIIa and FcγRIIIb[33], which have been shown to be key to AME of monocytes[15]. Additionally, afucosylated antibodies have been shown to correlate with COVID-19 disease severity as well as with inflammatory cytokine release by monocytes and macrophages[34,35]. Notably, patients vaccinated against COVID-19 did not show an increase in antibody afucosylation that was seen in patients with severe COVID-19, indicating that antibodies elicited by vaccination may avoid the risks associated with high levels of afucosylation[36].

2.3.3. AME of SARS-CoV-2 into various FcγRs for mAbs and serum

Several mAbs have been shown to enable Fcγ receptor (FcγR)-dependent antibody-mediated entry (AME) of SARS-CoV-2 into cells[1,16,17]. One study that characterized 48 mAbs isolated from a COVID-19 patient's serum found that 11 of them mediate FcγRII-dependent entry of SARS-CoV-2-spike-pseudotyped viral particles into Raji cells[17], which largely express FcγRIIb[16]. Another tested 100 anti-SARS-CoV-2-spike mAbs from a COVID-19 patient for FcγR-dependent entry of SARS-CoV-2-spike-pseudotyped viral particles into ACE2-negative TZM-bl cells[1]. The group identified five that mediated entry; of them, all mediated entry into FcγRIIb-expressing cells, and three mediated entry into FcγRI-expressing cells[1]. Recently, two mAbs from a COVID-19 patient that mediated FcγRIIb-dependent SARS-CoV-2-spike-pseudotyped viral particle entry into Raji cells were identified[16].

Additionally, work showing COVID-19 patient serum and plasma as both able[15,31,32,37] and unable[38] to mediate SARS-CoV-2 infection of FcγR-expressing cells have been published. In these studies, FcγRI[15], FcγRIIa[32,37], FcRIIb[31], and FcγRIII[15] have been identified as AME

receptors. Notably, two studies that saw the effect in patient serum found that 31%[32] and 40%[31] of patient serum tested mediated SARS-CoV-2 entry.

Why only some antibodies and patient serums can mediate FcγR-dependent entry is not fully understood. As described above, afucosylation[15] and epitope[17] have been implicated as potential differentiating antibody characteristics, and antibodies also seem to require bivalent interactions with the spike to mediate entry[16]. However, these factors do not fully address potential differences in allowing viral fusion, which has been shown to be required for AME[16]. In particular, it is unknown whether or how the conformational changes of the SARS-CoV-2 spike that are associated with viral fusion to ACE2-expressing cells[4] are involved in antibody-mediated viral fusion to FcγR-expressing cells.

2.4 SARS-CoV-2 spike conformational regulation

In the unbound prefusion conformation, the SARS-CoV-2 spike protein RBDs change between two conformational states: up, or open, where the ACE2 binding site is exposed, and down, or closed, where the ACE2 binding site is buried[12]. For unbound SARS-CoV-2 spike trimers, there is an equilibrium between a state with all three RBDs in the down conformation (3-down) and a state with two RBDs in the down conformation and one in the up conformation (1-up)[11,12].

Conformational dynamics, both in the spike RBD and the larger S1 and S2 subunits, are key to SARS-CoV-2 binding and fusion with host cells, and changes to these dynamics are therefore impactful to binding and entry[4]. Comparing the original SARS-CoV-2 variant with the later-dominant variants containing a D614G mutation, D614G causes increased energetic favorability for the 1-up spike trimer state[39]. Previous work has shown a range of relative populations of 3-down and 1-up states for unbound D614 spike trimers[11,40,41], but multiple have found approximately half of the unbound spike trimers each in the 3-down and 1-up states[11,41]. In

contrast, D614G trimers have been shown to strongly favor RBDs in the up conformation, with 87% of trimers in either the 2-up state, which is not observed for unbound D614 spike trimers, or

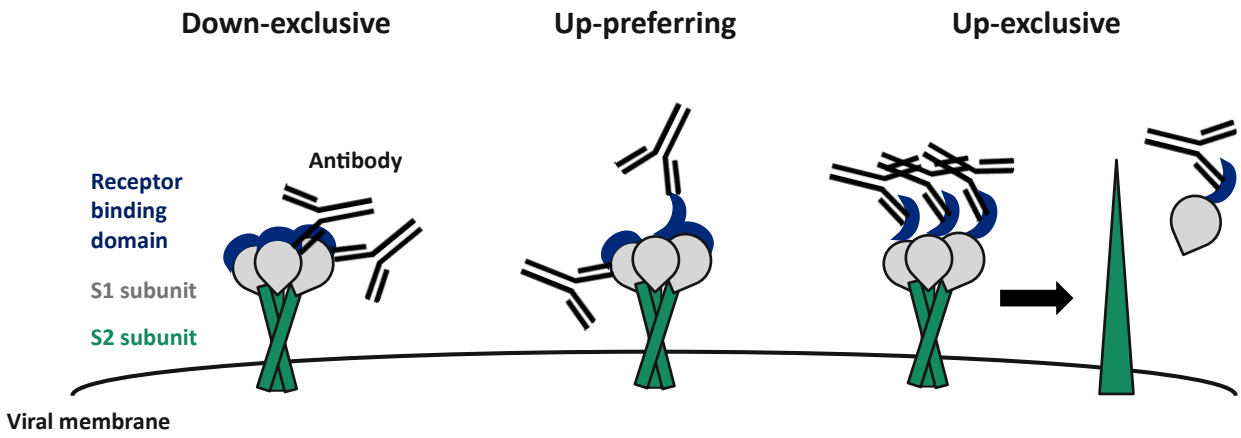

Figure 1. Conformational regulation of SARS-CoV-2 spike by monoclonal antibodies

the 1-up state[42]. More frequent sampling of the up conformation would be expected to increase access to the ACE2 binding site and subsequently increase viral binding and entry, which is reflected by *in vitro* studies showing a 1.3- to 4.6-fold increase in viral entry into various ACE2-expressing cells for D614G relative to D614[2,3]. The D614G mutation therefore demonstrates the critical role of RBD conformational dynamics on viral entry as measured *in vitro*. These differences in D614G also have *in vivo* and systemic implications given the rapid dominance of this mutation in circulating variants and increased viral load in patients infected with a D614G variant[3,43].

It has been shown that monoclonal antibodies (mAbs) that target the SARS-CoV-2 spike can affect the conformational dynamics of the spike in ways that likely affect antibody function **(Figure 1)**. Many antibodies that neutralize ACE2-mediated entry of SARS-CoV-2 are competitive inhibitors of ACE2, and similarly bind only the up conformation of the spike RBD **(Figure 1, right)** [5,6,8,18]. In addition to steric hindrance, these up-exclusive antibodies can neutralize ACE2 binding by similarly promoting the metastable bound 3-up state of the spike trimer[8,9]. With the exposure

of the S2 cleavage site in the 3-up state, the antibody-bound trimer is vulnerable to premature cleavage and dissociation of the S1 subunit, along with the bound antibody, and subsequent conformational changes into the postfusion state that cannot initiate binding or fusion[8]. In contrast, antibodies have been identified that bind only the down conformation of the RBD, making them down-exclusive antibodies that likely neutralize ACE2 entry by locking the spike in the 3-down state that cannot bind ACE2 **(Figure 1, left)** [5–7]. Additionally, some antibodies are up-preferring, shifting the spike trimer population toward states with at least one RBD in the up conformation but without explicitly up-exclusive binding **(Figure 1, center)** [1,5,16].

Notably, Wang et al. found that two AME mAbs could bind either the up or the down conformation of the spike RBD[16]. Similarly, the Li et al. study found that the FcγR-dependent AME antibodies they structurally characterized bind both the up and down conformations of the RBD[1]. The study also notes that the population of spike trimers was shifted such that all trimers were in a state with at least 1 RBD up, with none in the 3-down state, suggesting at least a weak preference for the up RBD conformation by these antibodies[1]. Whether this up-preferring binding is required for AME will be explored in this work, which investigates how SARS-CoV-2 spike conformational regulation by antibodies is related to their ability to mediate fusion and entry into FcγR-expressing cells.

Chapter III: Epitope and structure basis for antibody differences in SARS-CoV-2 conformational regulation and antibody-mediated entry

3.1 Introduction

A key effect of SARS-CoV-2 RBD conformational dynamics is periodic masking of the ACE2 binding site in the down conformation[12]. Many neutralizing antibodies, of which known AME antibodies are often a subset[16], compete for this site, making their epitopes inaccessible in the down conformation. One study classified 34 different antibodies and nanobodies targeting the SARS-CoV-2 ACE2 binding site into three epitope classes that also correspond with varying abilities to bind the up and down conformations of the SARS-CoV-2 RBD[44]. A similar study also identified epitopes on the ACE2 binding site that correlated with ability to bind the up and down conformations[45]. Given the connection between spike RBD conformational regulation and epitope, and the role of RBD conformational dynamics in viral entry[2–7], we hypothesize that certain antibody epitopes on the RBD will correlate with both RBD conformational regulation and ability to mediate entry into FcγR-expressing cells.

To investigate the relationships between antibody epitope, conformational regulation, and ability to mediate entry into FcγR-expressing cells, we conducted an analysis of previously published antibody-RBD structures with known conformational regulation, and some with known AME ability, to determine the location and accessibility of their epitopes in up and down RBD conformations for full spike trimer structures.

3.2 Materials and Methods

3.2.1 Epitope analysis

Structures for CV30 (PDB: 6XE1[8]), C105 (6XCM[46]), MW07 (7DK2[16]), DH1047 (7LD1[1]), DH1041 (7LAA[1]), DH1043 (7LJR[1]), MW01 (7DJZ[16]), MW05 (7DK0[16]), 2-4 (6XEY[17]), C144 (7K90[5]), and ACE2 (6M0J[47]) were all obtained from the Protein Data Bank (PDB). Antibodies that were found in their respective structures to bind only up or down RBDs were defined as "up-exclusive" and "down-exclusive," respectively. Antibodies that caused a shift in the trimer population away from the 3-down state but were not found to require the up state to bind were classified as "up-preferring." Some antibodies were classified as having "unknown" conformational regulation if the regulation of spike trimer conformations by that antibody was not clear. SARS-CoV-2 spike epitopes for antibody Fab fragments and ACE2 were defined as residues within 6 Å of the Fab or ACE2 and calculated using Pymol. Images of shared epitope residues on the RBD were generated using Chimera.

3.2.2 Clash analysis

Alignment of the original antibody structures to the clash analysis structures was performed using Pymol. Four clash analysis structures of SARS-CoV-2 spike with a D614G mutation were identified in the literature that represent the 4 possible spike trimer states: 3-down (PDB: 7KRQ[48]), 1-up (PDB: 7KRR)[48], 2-up (PDB: 7BNO[42]), and 3-up (PDB: 7WO5[49]). For each of the 3 chains (spike protomers) of each of these clash analysis structures, the RBD (residues 333-527[50]) was aligned to the RBD of the corresponding chain on the original antibody structure. For original antibody structures that contained fewer than 3 RBDs, as many RBDs as available were used throughout the analysis, but RBDs were aligned with multiple chains of the clash analysis structures as necessary. A new PDB containing only the clash analysis structure and the single aligned Fab fragment was thereby generated for each Fab/chain/trimer state combination. For

each new PDB, clashes were defined as van der Waals overlap ≥ 1 Å after subtracting 0.40 Å for H-bonding and quantified using Chimera.

3.3 Results

3.3.1 Epitope analysis of anti-SARS-CoV-2 antibody groups

From the literature, we identified neutralizing anti-SARS-CoV-2 mAbs previously analyzed by cryo-EM or crystallography[1,5,7,8,16,46]. From these structural data, we categorized the mAbs based on their conformational regulation of the SARS-CoV-2 RBD and ability to mediate AME **(Table 1)**. Antibodies with "up-exclusive" behavior (Group 1) were identified as those that were reported to bind only to up RBDs in cryo-electron microscopy (cryoEM) studies, while antibodies with "down-exclusive" behavior (Group 4) were defined as those that were found to bind only down RBDs in cryoEM. The one Group 1 antibody that had been previously tested for AME ability had not demonstrated any AME[16], and no Group 4 antibodies had previous been tested for AME ability. Groups 2, 3, and 5 were differentiated largely by their respective abilities to mediate entry into cells expressing FcγRI, FcγRIIb, or both. Their conformational regulation abilities were less defined by previous work than those of Groups 1 and 4, but Group 2 and Group 3 antibodies were previously shown to shift the spike trimer conformational equilibrium away from the 3-down state and toward a range of 1-, 2-, and 3-up states[1,16]. They were therefore classified as "up-preferring."

We then examined the published structures of each antibody described in Table 1 to identify their structural epitopes and compare similarities and differences in the antibody epitopes between and within each group. The groups which included more than one antibody (i.e., Groups 1, 3, and 4) each showed an intra-group overlap of residues shared among all antibody epitopes in the respective group. This epitope overlap ranged from 60.7% shared among all antibodies in Group

3 (17 shared residues out of 28 total residues for the smallest epitope in that group) to 95% shared for the antibodies in Group 4 (19 shared residues out of 20 total).

The shared epitopes for each group were then mapped onto the RBD and compared to the ACE2 epitope. The Group 1 epitope overlapped (18 residues) with over half of the ACE2 binding site (30 residues), with the majority of both the overlapping and non-overlapping (9 residues) Group 1 epitope residues lying on the inner face of the RBD that is hidden when the RBD is down. Given the up-exclusive binding of both ACE2 and the Group 1 antibodies, this shared epitope and high involvement of the inner face in binding are both expected. The Group 2 FcγRI AME antibody similarly bound the inner face, but had much less overlap (7 residues out of 37 total residues) with the ACE2 epitope, instead targeting below the ACE2 binding site. In contrast to the Group 1 and 2 antibodies, the Group 3 FcγRIIb AME antibody epitope had minimal involvement of the inner face, focusing instead on the top and outer faces. The Group 4 down-exclusive antibodies had a relatively similar epitope to that of Group 3 (10 shared residues). However, the Group 4 epitope had more overlap with the ACE2 binding site and the inner face (14/19 residues shared with ACE2) than the Group 3 epitope did (8/17 residues shared with ACE2), thereby involving the inner and top faces more and the outer face slightly less.

Notably, the shared epitopes for Groups 2 (37 residues) and 3 (17 residues), which mediate viral entry via FcγRI and FcγRIIb, respectively, had no overlap. The Group 2 epitope was also completely unique from the shared epitope of Group 4 (19 residues), which contains down-exclusive antibodies. The Group 1 epitope (27 residues) had some overlap (7 residues) with the Group 2 epitope (37 residues) but overlapped more (18 residues) with the epitope of ACE2 (30 residues). The Group 5 antibody, DH1046, which mediates entry via both FcγRI and FcγRIIb[1], did

not have an existing structure, but was found to compete with Group 2 AME antibody DH1047[1], indicating that there is some overlap between their epitopes.

Table 1. Unique antibody epitopes are associated with different conformational and AME effects for SARS-CoV-2.

		Grouped by						
mAb Group	mAb Name	Conformational Regulation	AME	PDB ID	Heavy/Light Chain Subclass[1]	Neutralizing?	# shared group residues/# total epitope residues	Location of shared residues on RBD (vs. ACE2 site[2])
1	CV30	Up-exclusive[3a]	Unknown[d]	6XE1[3]	IGHV3-53, IGKV3-20[3]	Yes[3]	27/38	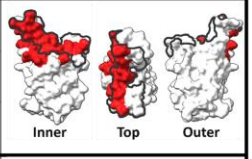
	C105	Up-exclusive[4]	Unknown[d]	6XCM[4]	IGHV3-53, IGLV2-8[4]	Yes[5]	27/34	
	MW07	Up-exclusive[6]	None[6]	7DK2[6]	IGHV3-7, IGKV1-NL1[6]	Yes[6]	27/46	
2	DH1047	Up-preferring[7b]	FcγRI[7]	7LD1[7]	IGHV1-46, IGKV4-1[7]	Yes[7]	Unknown/37	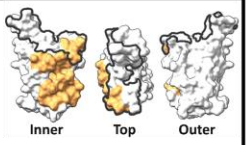
3	DH1041	Up-preferring[7]	FcγRIIb[7]	7LAA[7]	IGHV3-7, IGLV1-40[7]	Yes[7]	17/28	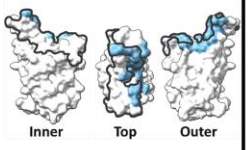
	DH1043	Up-preferring[7]	FcγRIIb[7]	7LJR[7]	IGHV1-69, IGKV3-20[7]	Yes[7]	17/33	
	MW01	Unknown	FcγRIIb[6]	7DJZ[6]	IGHV1-69, IGKV3-15[6e]	Yes[6]	17/31	
	MW05	Unknown	FcγRIIb[6]	7DK0[6]	IGHV1-69, IGKV3-15[6e]	Yes[6]	17/32	
4	2-4	Down-exclusive[8c]	Unknown[d]	6XEY[8]	IGHV1-2, IGLV2-8[8]	Yes[8]	19/20	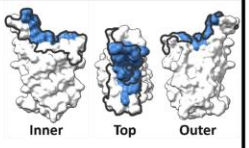
	C144	Down-exclusive[9]	Unknown[d]	7K90[9]	IGHV3-53, IGLV2-14[9]	Yes[5]	19/27	
5	DH1046	Unknown	FcγRI and FcγRIIb[7]	n/a	IGHV3-23, IGKV1-5[7]	Yes[7]	Unknown	Unknown

[a] requires up RBD conformation to bind
[b] shifts equilibrium of spike trimers away from 3-down state, but does not definitively require up RBD conformation to bind
[c] requires down RBD conformation to bind
[d] to our knowledge, demonstrated for the first time in this work (See Figure 4, Table 2)
[e] while these antibodies have the same variable (V) genes, as shown, they have unique heavy and light joining (J) genes[1]

1. Raybould, M. I. K. et al. *Bioinformatics* (2021)
2. Lan, J. et al. *Nature (2020)*
3. Hurlburt, N. K. et al. *Nat. Commun.* (2020)
4. Barnes, C. O. et al. *Cell* (2020)
5. Robbiani, D. F. et al. *Nature* (2020)
6. Wang, S. et al. *Commun Biol* (2022)
7. Li, D. et al. *Cell* (2021)
8. Liu, L. et al. *Nature* (2020)
9. Barnes, C. O. et al. *Cell* (2020)

3.3.2 Analysis of steric clashing for anti-SARS-CoV-2 antibodies aligned with spike trimers

To investigate whether there was a structural basis for these differences in epitope and conformational regulation ability among the antibody groups, we aligned each antibody to baseline spike structures representing the 4 possible trimer states (i.e., 3-RBD-down, 1-up, 2-up, and 3-up) **(Figure 2A-B)**. After aligning the antibodies to each RBD on the 4 spike structures, we quantified the resulting steric clashes for each antibody-RBD alignment, averaging the number of clashes within each group **(Figure 2C-D)**. For all Group 1 antibodies, which only bind the up conformation, the number of clashes were uniformly high when aligned to down RBDs, ranging from 1599 to 3904 clashes, and uniformly low when binding up RBDs, ranging from 6 to 35 clashes. This thermodynamic unfavorability of binding the down conformation supports the structural and epitope data for antibodies in this group. Similarly, the Group 2 antibody that mediates FcγRI AME had a high number of clashes when aligned to RBDs in the down conformation, ranging from 886 to 2795 clashes, and had very few clashes with RBDs in the 3-up state (36 to 91 clashes). However, in contrast to the Group 1 antibodies, there were as many as 360 and 250 steric clashes for the Group 2 antibody when aligned to up RBDs in 1-up or 2-up trimers, respectively, with clashes located largely with an adjacent down conformation. Notably, the original structure of this Group 2 antibody was in the 3-up state, indicating that antibody binding to the 3-up state is allowable[1]. We therefore concluded that a clash number under 91, which was found when aligning this antibody to the 3-up state, would be resolved by normal movement of atoms and sidechains when the antibody aligns and binds to a moving, rather than static, protein structure. In contrast, we expect that a larger number of clashes (i.e. greater than ~100 clashes) would only be resolved by larger protein movements that may not be thermodynamically favored or even structurally feasible.

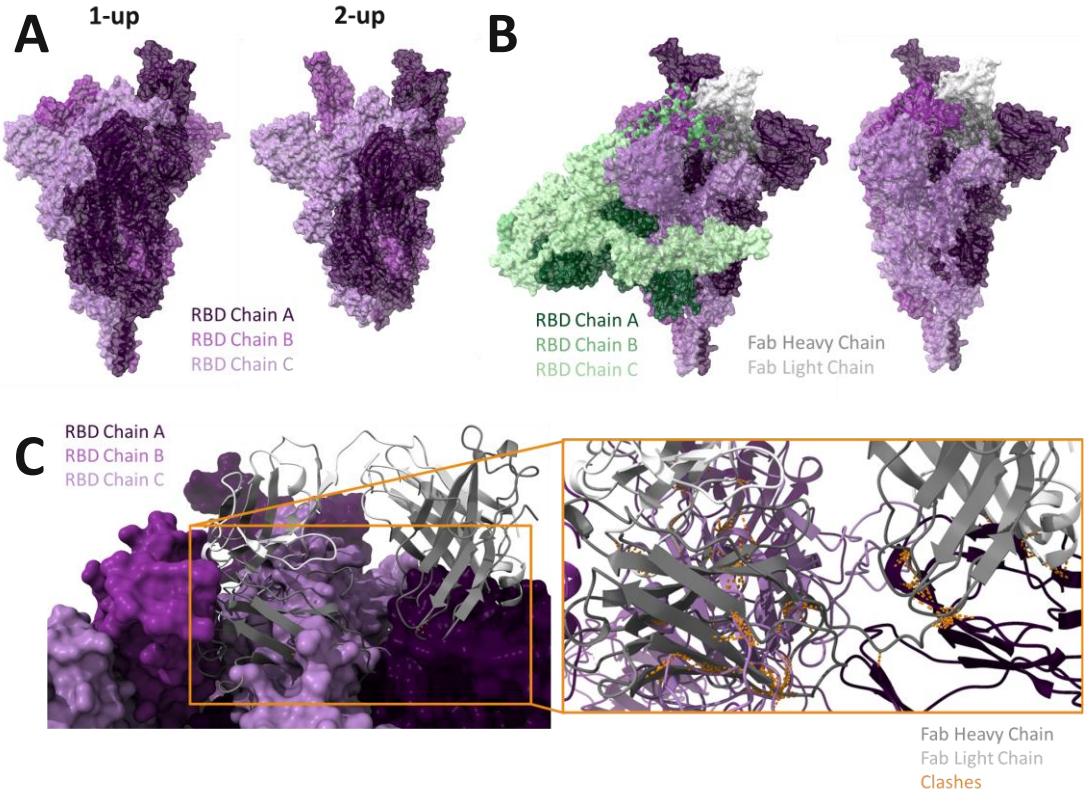
A
1-up
2-up
RBD Chain A
RBD Chain B
RBD Chain C
B
RBD Chain A
RBD Chain B
RBD Chain C
Fab Heavy Chain
Fab Light Chain
C
RBD Chain A
RBD Chain B
RBD Chain C
Fab Heavy Chain
Fab Light Chain
Clashes
D
RBD Chain A
RBD Chain B
RBD Chain C
Clash Number
5000
4000
3000
2000
1000
0
3-down
1-up
2-up
3-up
Group 1
CV30
C102
C105
MW07
Group 2
DH1047
Group 3
DH1041
DH1043
MW01
MW05
Group 4
2-4
C144

Figure 2. Quantified steric clashes for anti-SARS-CoV-2 antibody binding support group conformational regulation characteristics.
(A) Structures of 1-up (left, PDB: 7KRR[48]) and 2-up (right, PDB: 7BNO[9]) states of SARS-CoV-2 spike trimer used for clash analysis, showing that in the 1-up state, only Chain A is up and in the 2-up state, Chains A and B are up. **(B)** Representative images showing RBD-only (residues 333-527[39]) alignment of original antibody-containing structure (green, PDB: 6XCM[46]) and structure for clash analysis (purple, PDB: 7KRR [48]). After alignment of RBDs (left), antibody Fab fragment (gray) is aligned with down RBD of clash analysis structure (right), despite original structure being in the up conformation. **(C)** Representative images showing identification of clashes (orange), defined as van der Waals overlap ≥ 1 Å after subtracting 0.40 Å for H-bonding. Right image shows zoomed in ribbon structure of indicated section of left image. **(D)** Graph of average ± standard deviation of clashes for each antibody group in Table 1.

3.4 Discussion

While previous work has identified epitope regions on the RBD and associated them with up-exclusive and down-exclusive binding[44,51], such shared epitopes have to our knowledge not previously been defined for AME antibodies, which also demonstrate unique conformational regulation behavior[1]. Additionally, the structural epitope analysis shown in this work suggests not only that certain mAb epitopes are associated with AME in general, but that antibodies mediating entry via different FcγRs also bind unique epitopes on the RBD. This work ultimately indicates that AME, conformational regulation, and epitope for anti-SARS-CoV-2 mAbs are both connected and predictive.

This connection between epitope, conformational regulation, and AME could be applied to vaccine antigen design for COVID-19 and related viral diseases. By mutating these epitope regions specific to AME, vaccine antigens could be designed to elicit only antibodies that neutralize viral entry, without enabling AME into FcγR-dependent cells. Notably, mutations targeting the Group 2 AME epitope, which is largely on the inner face, would need to be selected carefully to avoid destabilizing RBD conformational dynamics or the spike structure overall. However, strategic individual mutations to the SARS-CoV-2 RBD, including on the inner face, have been shown to eliminate binding of specific antibodies while retaining infection ability of the virus overall[52], suggesting that this approach could be feasible.

It is important to note that the structural analysis and the correlations between antibody epitope, AME ability, and conformational regulation described in this work are based on a relatively small number of antibodies for each group, particularly Group 2. Structurally, the Group 2 antibody binds a region on the epitope that has minimal overlap with the ACE2 binding site (7 residues out of 37 total residues)[1] and does not fit clearly into previously defined epitope classes[44,51]. As a result, it is challenging to identify potential Group 2 antibodies among the many anti-SARS-CoV-2 antibodies that have been structurally characterized. Functionally, nearly all mAbs that have been found to mediate SARS-CoV-2 entry into FcγR-expressing cells do so via FcγRIIb[1,16,17], which is minimally expressed on monocytes and macrophages that have been implicated in COVID-19 inflammation[15]. Wider testing for antibodies that mediate FcγRI entry, which is more likely to be involved in monocyte and macrophage infection[15,53], would support identification of additional Group 2 antibodies. Nevertheless, the Group 2 epitope does partially overlap with mAb CR3022 (17/37 residues shared), and a number of antibodies have been found compete with CR3022[52]. Although these antibodies have not been structurally characterized at a high resolution, mutational analysis does provide information about their epitope[52]. Therefore, testing these antibodies for potential FcγRI-mediated entry is an immediate future direction for our group that may allow us to add additional antibodies to the analyzed set.

Overall, identification and analysis of additional antibodies, particularly those that mediate entry via FcγRI, that have known structures and epitopes would allow for greater confidence in defining inclusive and exclusive criteria for the antibody groups. Even within groups that contain more than one member, there are variations in binding angle, number of clashes, and epitope among the antibodies that make it challenging to confidently identify the defining characteristics of each group. An unbiased clustering analysis of the antibodies that considers these factors, particularly

epitope, would also help provide additional confidence in the definition of the antibody groups. In addition, while the structural epitopes described in Table 1 indicate a region on the RBD where the mAbs bind, experimental studies including mutational analysis would be necessary to identify specific residues on the RBD that are functionally required for initiating AME and further define the requirements of each antibody group.

Chapter IV: Neutralization and antibody-mediated entry ability for anti-SARS-CoV-2 antibodies of different groups

4.1 Introduction

FcγR-mediated SARS-CoV-2 infection has been detected in both monocytes[15] and tissue-resident macrophages[15] from COVID-19 patients. While SARS-CoV-2 infection of FcγR-expressing cells is known to be abortive, not leading to replication of live virus inside the cell [15,22], infection with the virus has been shown to cause increased release of inflammatory cytokines, such as TNF and IL-6[22], inflammasome activation[15], and cell death[15,22], notably pyroptosis associated with inflammation[15], in these cell types. Because these inflammatory effects have also been shown to correlate with COVID-19 disease severity[15], understanding what allows some, but not all, antibodies to mediate AME and these subsequent downstream effects remains important to improving treatment for COVID-19 patients.

Based on the key role of RBD conformational dynamics on SARS-CoV-2 viral entry[2–7], we propose a model for FcγR-dependent AME of SARS-CoV-2 that connects ability to mediate entry to effect on RBD conformational dynamics **(Figure 3)**. We hypothesize that spike/antibody complex binding to FcγR while in the activated 3-up state, but prior to S1 subunit shedding, is critical to facilitate fusion of the viral and cell membranes and subsequent release of the viral genome into the cell cytoplasm. Without stabilization of the 3-up state, we anticipate that viruses will be destroyed in endosomes without releasing their genome into the cytoplasm. If the S1 subunits are shed prior to FcγR binding, the spike will have transitioned into the binding-incompetent postfusion conformation, becoming unable to bind and fuse with host cells. We therefore

hypothesize ability, or lack of ability, to mediate entry into FcγR-expressing cells correlates with the following conformational types:

1. **Up-selective antibodies** that stabilize the up conformation of the RBD, for which we classify two subtypes:

   1a. Up-exclusive antibodies that only bind the up RBD conformation, and therefore strongly promote the metastable prefusion 3-RBD-up spike state and subsequent shedding of the S1 subunit prior to FcγR binding. We hypothesize that up-exclusive antibodies will not induce AME.

   1b. Up-preferring antibodies that shift the spike trimer equilibrium toward states with RBDs in the up conformation, but do so more moderately than up-exclusive antibodies do. We predict these antibodies shift the population of spike trimers to have more up RBDs, which are necessary for fusion, but less strongly than those that induce premature S1 subunit shedding. We hypothesize that up-preferring antibodies will induce AME.

   Why certain antibodies mediate entry via some FcγRs, but not others, is also unknown. However, notably, FcγRI and FcγRIIb, two known AME receptors, differ in their respective affinities for the Fc fragment of antibodies, with FcγRI being having high affinity and FcγRIIb having low to medium affinity[54]. It is possible that differences in epitope, binding angle, and subsequent avidity for certain antibodies and antibody-virus complexes leads to differences in FcγR binding and entry among these up-preferring antibodies[55].

2. **Down-exclusive antibodies** that only bind to the down RBD conformation and therefore promote the 3-down state, which we predict will not allow exposure of the S2' cleavage site and therefore will prevent fusion after FcγR binding. We hypothesize that down-exclusive antibodies will not induce AME.

The ability of up-exclusive and down-exclusive antibodies to mediate FcγR-dependent entry has not been deeply investigated. Therefore, in order to investigate this proposed connection between

antibody RBD conformational regulation and ability to mediate entry, we used a lentiviral pseudovirus system to test antibodies with known conformational regulation for their ability to mediate entry into FcγRI-expressing THP1-derived macrophages.

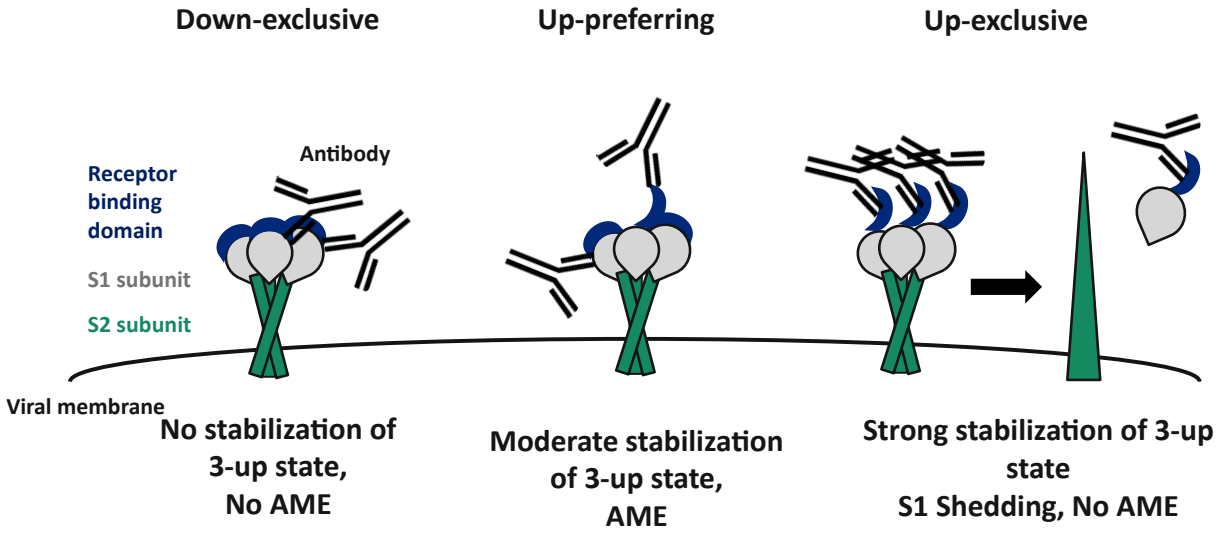

Figure 3. Proposed relationship between SARS-CoV-2 RBD conformational dynamics and antibody-mediated entry (AME)

4.2 Materials and Methods

4.2.2 Production of SARS-CoV-2-spike-pseudotyped lentiviral particles

Non-replicative HIV-1-derived lentiviral particles pseudotyped with SARS-CoV-2 spike were produced as previously described[56]. In brief, human embryonic kidney (HEK) 293T cells were co-transfected with five plasmids: one containing the lentiviral backbone and reporter proteins (BEI catalog number NR-52516), three for key HIV-1 proteins (Tat (NR-52518), Gag-Pol (NR-52517), and Rev (NR-52519)), and one encoding the entry protein. To produce SARS-CoV-2-spike-pseudotyped viral particles, the entry protein plasmid that was used encoded a SARS-CoV-2 spike variant containing a C-terminal 21-amino-acid deletion and a D614G mutation (NR-53765). For positive and negative control pseudoviruses, an HDM-VSVG plasmid encoding VSV G and a

transfection carrier plasmid (Promega), respectively, were instead used as the entry protein plasmid. Transfections were performed using Lipofectamine 2000 (Invitrogen) according to manufacturer's protocols. All resulting lentiviruses contained luciferase expressed with a CMV primary promoter and fluorescent ZsGreen expressed with an internal ribosome entry site (IRES). Following a 72-hour transfection using Lipofectamine, supernatant was filtered through a 0.45 µm SFCA low-protein-binding filter to harvest the pseudoviruses. Prior to transfection, HEK cells were cultured in Dulbecco's Modified Eagle Medium (DMEM, Gibco) with 10% heat-inactivated FBS (R&D Systems), 100 U/mL Pen-Strep (Gibco), and 2 mM L-glutamine (Gibco). For the transfection, cells were switched to RPMI (Gibco) with 10% heat-inactivated FBS (R&D Systems), 100 U/mL Pen-Strep (Gibco), 1 mM sodium pyruvate (Gibco), and 2 mM L-glutamine (Gibco). All cell culture and experiment incubation steps described in this work were performed at 37°C with 5% CO_2.

4.2.3 Measuring antibody-mediated neutralization of pseudovirus entry into ACE2-expressing cells

Measurement of viral entry into ACE2-expressing cells was measured as previously described[56]. Briefly, tissue-culture-treated 96-well plates were seeded with either 293T or 293T-ACE2 cells (~25,000 cells/well) approximately 16 hours before infection with pseudovirus. For all pseudovirus infections described in this work, pseudovirus was added at a 2:3 dilution in fresh media, with a total infection volume of 150 µL per well. Pseudoviruses were preincubated with varying concentrations of mAbs for 1 hour before being added to the seeded cells allowed to infect the cells for 50 hours. Three wells for each antibody concentration were used in each biological replicate. Following the infection period, pseudovirus-containing media in each well was replaced with 100 µL of fresh phenol-red-free DMEM (Gibco) with 2 mM DMNPE-caged luciferin (GoldBio).

Luminescence measurements were taken as frequently as possible over approximately 5 minutes following addition of luciferin. Decrease in luminescence in this assay indicates neutralization. For incubation steps described in this section, cells and pseudoviruses were cultured and incubated at 37°C with 5% CO_2. Media used for this section was DMEM with 10% heat-inactivated FBS (R&D Systems), 100 U/mL Pen-Strep (Gibco), and 2 mM L-glutamine (Gibco). Data for each antibody were fit to a nonlinear regression [inhibitor] vs. response model with three parameters and graphed using GraphPad Prism. These fits were used to calculate neutralization IC_{50}, defined as the concentration required to reach 50% inhibition of the entry with no antibody, which was calculated for each biological replicate.

4.2.4 Measuring antibody-mediated pseudovirus entry into FcγR-expressing cells

In order to measure antibody-mediated pseudoviral entry into macrophages, suspended THP-1 monocytes were differentiated into adherent macrophages using a method modified from one previously described[53]. Briefly, 300 of cells at 600,000 cells/mL with 7.5% phorbol-12-myristate 13-acetate (PMA) was added per well to tissue-culture-treated, white-walled 96-well plates (Corning) and incubated for 24 hours. Six wells were used for each antibody concentration per biological replicate. Following this PMA priming step, cells were washed once with DPBS before being rested with fresh media for 24 hours prior to pseudoviral infection. Media used for these cells was RPMI with 10% heat-inactivated FBS (R&D Systems), 100 U/mL Pen-Strep (Gibco), 1 mM sodium pyruvate (Gibco), and 2 mM L-glutamine (Gibco).

As described above for the neutralization assay, pseudoviruses were incubated with mAbs at varying concentrations for 1 hour before being added to the FcγR-expressing macrophages. Following a 48-hour infection incubation, pseudovirus entry into the cells was measured using luminescence, as described above. Luminescence readings were taken as often as possible over

approximately 6 minutes following the addition of luciferin; readings at approximately 30 seconds, 2 minutes and 30 seconds, and 4 minutes and 30 seconds were averaged for each well on each day. Increase in luminescence for this assay indicates AME. Data were analyzed using a two-way ANOVA with a post hoc Dunnett's test and graphed using GraphPad Prism.

4.3 Results

4.3.1. Neutralization of entry into ACE2-expressing cells

A subset of the antibodies described in Table 1 were then tested to directly compare their relative ability to neutralize SARS-CoV-2-spike-pseudotyped lentiviral particle entry into HEK 293T-ACE2 cells using one shared pseudovirus-cell system. As demonstrated in previous work, all tested antibodies neutralized pseudovirus entry into the 293T-ACE2 cells **(Figure 4A)**. Notably, the neutralization IC_{50}s of DH1046 (0.65 μg/mL) and DH1047 (1.60 μg/mL), the AME antibodies, were both higher than the IC_{50}s of each of the non-AME antibodies (0.0074 to 0.22 μg/mL), which also supports previously published neutralization data.

4.3.2. Antibody-mediated entry into THP1-derived macrophages

Given the previously demonstrated relationships between monocyte and macrophage SARS-CoV-2 infection, inflammatory cytokine release and cell death, and COVID-19 disease severity[15], we tested the panel of antibodies for their ability to mediate entry into THP1-derived macrophages **(Figure 4B-E).** Both DH1047 (Group 2) and DH1046 (Group 5) mediated statistically significant entry of the spike pseudovirus into THP1-derived macrophages compared to the same-day no antibody condition **(Figure 4B)**. These results therefore support previous work showing AME by DH1047 and DH1046 mAbs into FcγRI-expressing TZM-bl cells[1], and are expected given that THP1-derived macrophages have been shown to express FcγRI but only minimally express FcγRIIb[53]. To our knowledge, none of the tested Group 1 or Group 4 antibodies had previously

been tested for AME ability. We found that none of them showed any significant AME into the THP1-derived macrophages **(Figure 4C, 4E)**, which allowed us to update **Table 1** with additional information about these antibodies **(Table 2)**. Additionally, as expected based on prior work[1], neither DH1043 nor DH1041 (Group 3) mediated significant AME into the THP1-derived macrophages **(Figure 4E)**. Due to day-to-day variability in AME signal, sample data from a single

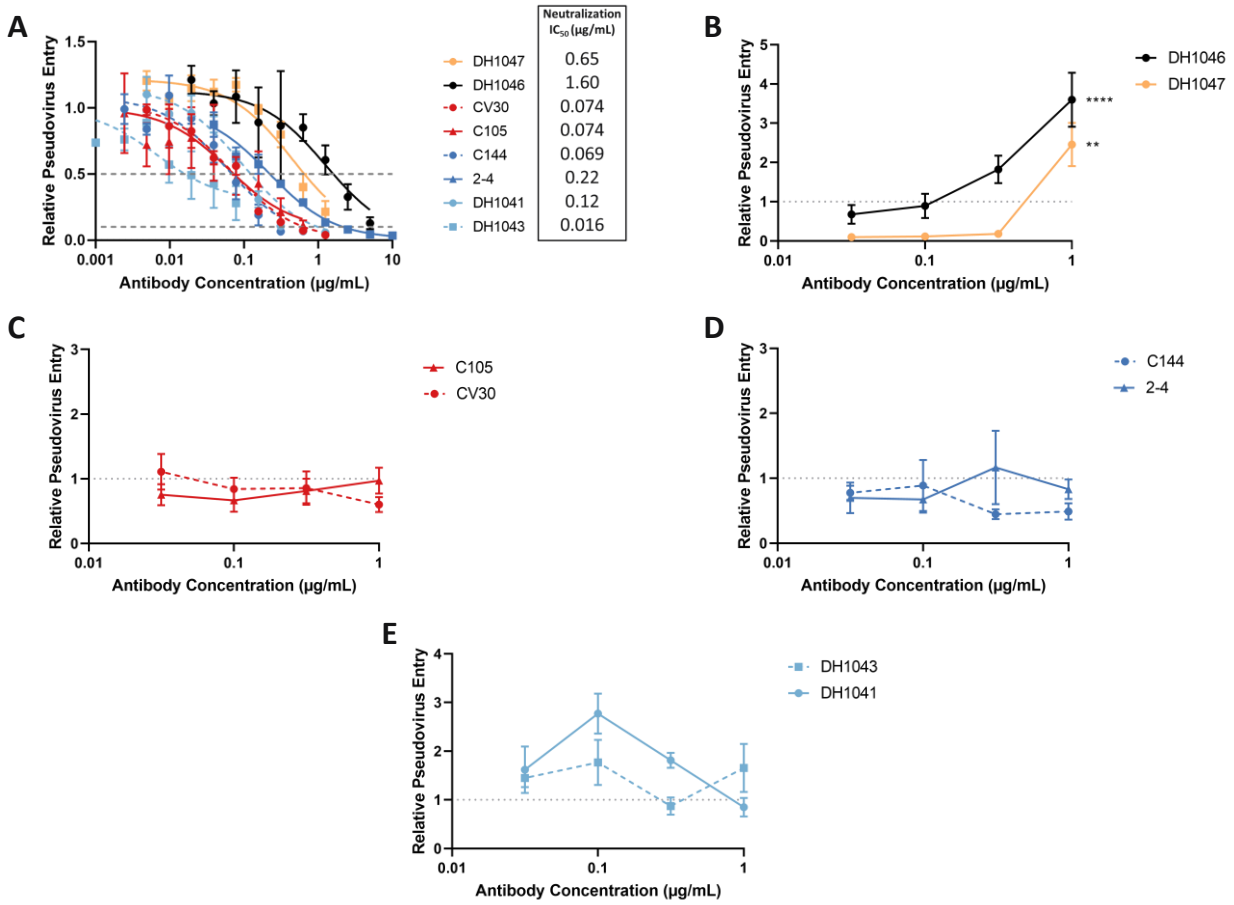

Figure 4. Anti-SARS-CoV-2 neutralizing antibodies of different groups have varying ability to mediate entry into THP1-derived macrophages.
Entry of SARS-CoV-2-spike-pseudotyped viral particles in the presence of varying concentrations of antibody normalized to entry of virus alone. **(A)** Neutralization of entry of pseudoviral particles into 293T-ACE2 HEK cells by mAbs. Lines for each antibody represent three-parameter nonlinear regression fit performed in Prism. Grey lines represent 50% (top) and 90% (bottom) inhibition of viral entry, respectively, with no mAb. Neutralizing IC_{50} for each antibody also shown. **(B-E)** Sample data showing average ± SEM AME into THP1-derived macrophages for 6 technical replicates each. ** represents $p \leq 0.01$ and **** represents $p \leq 0.0001$ for two-way ANOVA with post hoc Dunnett's test. Presence or absence of AME shown for each antibody was repeated in all biological replicates. Grey line represents amount of entry for virus alone.

biological replicate is shown for each antibody in Figure 4, but all biological replicates of these AME experiments showed the same results, with statistically significant AME shown only for DH1046 and DH1047 **(Figure 5)**.

Table 2. Updated version of Table 1 - Antibody epitopes are associated with different conformational and AME effects for SARS-CoV-2.

Grouped by

mAb Group	mAb Name	Conformational Regulation	AME	PDB ID	Heavy/Light Chain Subclass[1]	Neutralizing?	# shared group residues/# total epitope residues	Location of shared residues on RBD (vs. ACE2 site[2])
1	CV30	Up-exclusive[3a]	None[d]	6XE1[3]	IGHV3-53, IGKV3-20[3]	Yes[3]	27/38	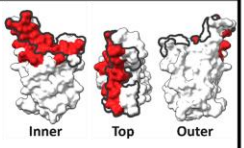
	C105	Up-exclusive[4]	None[d]	6XCM[4]	IGHV3-53, IGLV2-8[4]	Yes[5]	27/34	
	MW07	Up-exclusive[6]	None[6]	7DK2[6]	IGHV3-7, IGKV1-NL1[6]	Yes[6]	27/46	
2	DH1047	Up-preferring[7b]	FcγRI[7]	7LD1[7]	IGHV1-46, IGKV4-1[7]	Yes[7]	Unknown/37	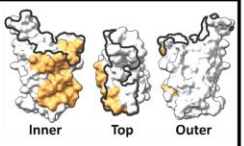
3	DH1041	Up-preferring[7]	FcγRIIb[7]	7LAA[7]	IGHV3-7, IGLV1-40[7]	Yes[7]	17/28	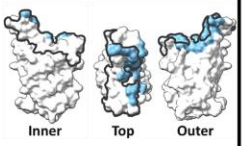
	DH1043	Up-preferring[7]	FcγRIIb[7]	7LJR[7]	IGHV1-69, IGKV3-20[7]	Yes[7]	17/33	
	MW01	Unknown	FcγRIIb[6]	7DJZ[6]	IGHV1-69, IGKV3-15[6e]	Yes[6]	17/31	
	MW05	Unknown	FcγRIIb[6]	7DK0[6]	IGHV1-69, IGKV3-15[6e]	Yes[6]	17/32	
4	2-4	Down-exclusive[8c]	None[d]	6XEY[8]	IGHV1-2, IGLV2-8[8]	Yes[8]	19/20	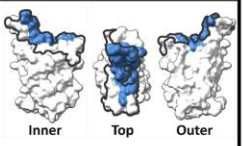
	C144	Down-exclusive[9]	None[d]	7K90[9]	IGHV3-53, IGLV2-14[9]	Yes[5]	19/27	
5	DH1046	Unknown	FcγRI and FcγRIIb[7]	n/a	IGHV3-23, IGKV1-5[7]	Yes[7]	Unknown	Unknown

[a] requires up RBD conformation to bind
[b] shifts equilibrium of spike trimers away from 3-down state, but does not definitively require up RBD conformation to bind
[c] requires down RBD conformation to bind
[d] to our knowledge, demonstrated for the first time in this work (See Figure 4, Table 2)
[e] while these antibodies have the same variable (V) genes, as shown, they have unique heavy and light joining (J) genes[1]

1. Raybould, M. I. K. et al. *Bioinformatics* (2021)
2. Lan, J. et al. *Nature (2020)*
3. Hurlburt, N. K. et al. *Nat. Commun.* (2020)
4. Barnes, C. O. et al. *Cell* (2020)
5. Robbiani, D. F. et al. *Nature* (2020)
6. Wang, S. et al. *Commun Biol* (2022)
7. Li, D. et al. *Cell* (2021)
8. Liu, L. et al. *Nature* (2020)
9. Barnes, C. O. et al. *Cell* (2020)

4.4 Discussion

To our knowledge, spike conformational regulation by mAbs has not previously been connected to ability or lack of ability to mediate entry into FcγR-expressing cells. Here, we found that, as hypothesized, up-exclusive and down-exclusive mAbs do not mediate viral entry. As also hypothesized, we found that, in contrast, antibodies that prefer the up conformation, but have not been shown to require it[1], are able to mediate entry into macrophages, which supports prior work showing FcγR-dependent entry for up-preferring antibodies[1,16]. This work therefore supports our hypothesis that requirement of the up RBD state to initiate fusion[9] prevents down-exclusive antibodies from mediating entry. We hypothesize that up-exclusive antibodies do, in contrast, promote this required 3-up state. However, prior work indicates that these up-exclusive antibodies can lead to premature cleavage and irreversible shedding of the RBD-containing S1 subunit from the virus[8]. It seems likely that this irreversible S1 subunit shedding could be occurring prior to viral binding, thereby preventing these antibodies from being able to mediate entry, which is reflected in the lack of AME for Group 1 antibodies. In contrast, up-preferring antibodies that may more slowly and less dramatically shift the equilibrium toward the up state could allow the antibodies time to connect the virus to the FcγR-expressing cells and initiate binding and subsequent AME without inducing premature S1 subunit shedding.

Notably, the antibodies and structures analyzed and tested in this work were generated from early variants of the SARS-CoV-2 virus, but the virus and its spike protein have continued to gain mutations and change over the course of the pandemic[57]. It is important to consider whether and how these mutations change the binding, neutralization, and AME characteristics that have been demonstrated for these antibody groups. For example, mutations present in the Omicron variant have been associated with greater favorability of the up RBD conformation[42], increased S1 cleavage[57], and greater affinity for ACE2[57]. Given the hypothesized key role of up conformation

stabilization without inducing premature S1 subunit shedding in AME, these mutations could alter which antibodies are able to effectively mediate FcγR-dependent entry. Mutations known to be present in the Omicron variant[57] are spread among the epitopes of all the antibody groups defined in this work. Therefore, AME and non-AME antibodies developed earlier in the pandemic may both bind more poorly to the Omicron variant, which does not clearly favor or disfavor AME. However, additional AME studies using virus pseudotyped with more recent spike variants and mutational studies identifying residues critical to AME antibody binding would provide more insight into how these antibody groups change in binding, neutralization, and AME ability with variants of SARS-CoV-2.

4.5 Supplementary Information

4.5.1 Supplementary Figures

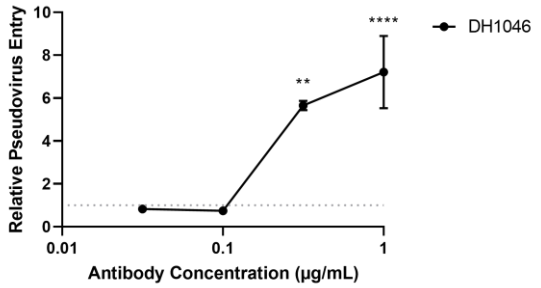
Relative Pseudovirus Entry
Antibody Concentration (μg/mL)
DH1046
****
**

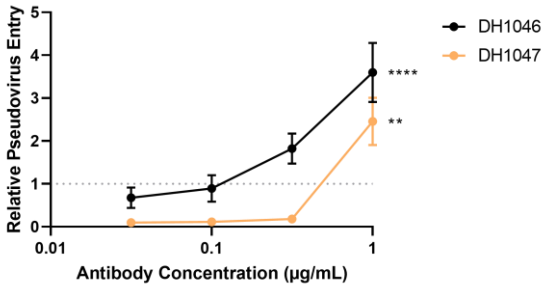
Relative Pseudovirus Entry
Antibody Concentration (μg/mL)
DH1046
DH1047
****
**

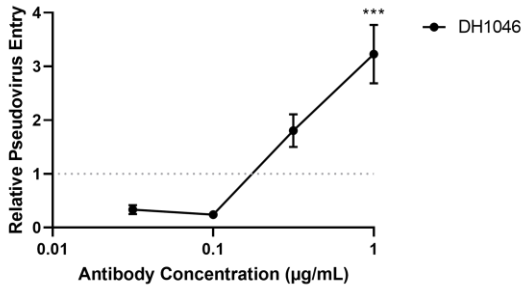
Relative Pseudovirus Entry
Antibody Concentration (μg/mL)
DH1046
***

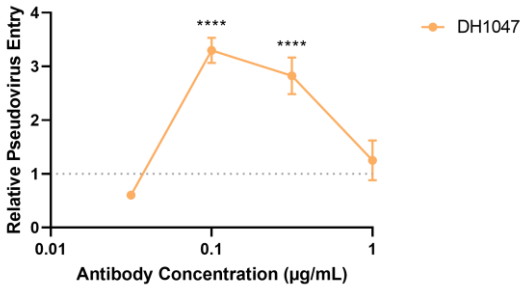
Relative Pseudovirus Entry
Antibody Concentration (μg/mL)
DH1047
****
****

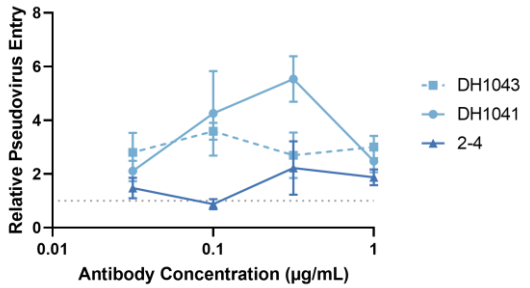
Relative Pseudovirus Entry
Antibody Concentration (μg/mL)
DH1043
DH1041
2-4

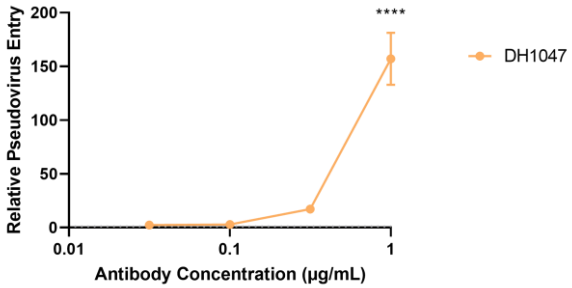
Relative Pseudovirus Entry
Antibody Concentration (μg/mL)
DH1047
****

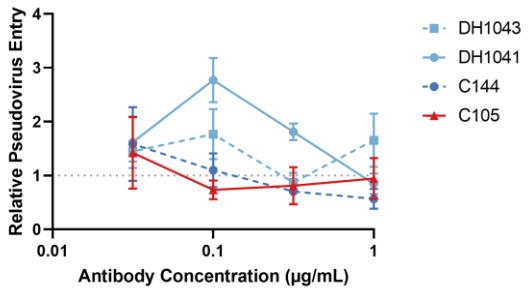
Relative Pseudovirus Entry
Antibody Concentration (μg/mL)
DH1043
DH1041
C144
C105

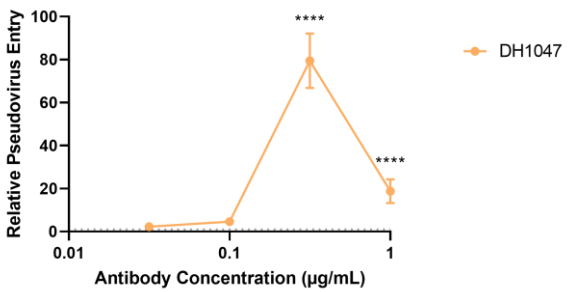
Relative Pseudovirus Entry
Antibody Concentration (μg/mL)
DH1047
****
****

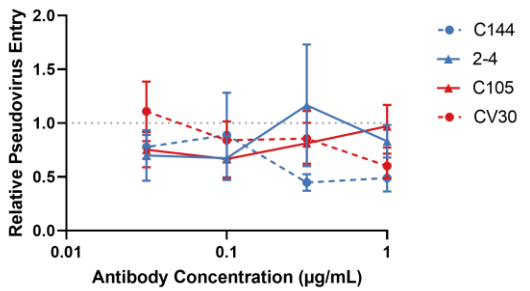
Relative Pseudovirus Entry
Antibody Concentration (μg/mL)
C144
2-4
C105
CV30

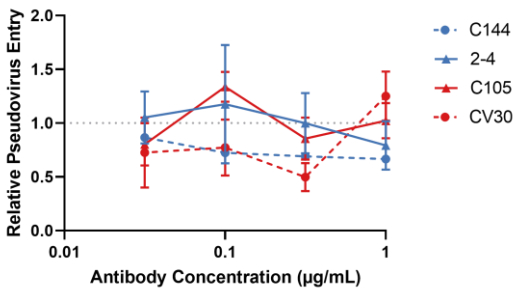
Relative Pseudovirus Entry
Antibody Concentration (μg/mL)
C144
2-4
C105
CV30

Figure 5. Biological replicate data showing AME into THP1-derived macrophages by DH1046 and DH1047 only. Entry of SARS-CoV-2-spike-pseudotyped viral particles in the presence of varying concentrations of antibody normalized to entry of virus alone (grey line). Points represent average ± SEM AME into THP1-derived macrophages for 6 technical replicates each. ** represents $p \leq 0.01$, *** represents $p \leq 0.001$, and **** represents $p \leq 0.0001$ for two-way ANOVA with post hoc Dunnett's test. Green boxes indicate data was collected in the same experiment.

Chapter V: Antibody inhibition of SARS-CoV-2 AME

5.1 Introduction

Given the role of AME in macrophage and monocyte infection, inflammatory cytokine release, and cell death[15] in COVID-19 patients, preventing this effect in patient antibody responses to infection and vaccination could reduce cytokine storms and subsequent disease severity and treatment side effects for COVID-19. Addressing this inflammatory effect would offer a new approach to treating COVID-19; existing vaccines and treatments, which primarily address viral load by neutralizing entry into ACE2-expressing cells, largely have limited effect once patients have been hospitalized with severe symptoms[58] largely driven by inflammatory cytokine storm[13,14]. Inhibiting AME may offer an additional mechanism of decreasing COVID-19 disease severity by limiting the inflammatory effects of SARS-CoV-2 expression of FcγR-expressing cells. Given the diversity of RBD conformational effects for mAbs, understanding how effective various conformational and competitive mechanisms are at inhibiting AME could support future vaccine and therapeutic design for COVID-19.

To determine the relative AME inhibition capabilities of several types of potential inhibitors, we used the pseudoviral AME assay described in Chapter IV with known AME antibodies in combination with antibodies that we anticipate will either conformationally or competitively inhibit entry.

5.2 Materials and Methods

5.2.1 Inhibition of AME into THP1-derived macrophages

AME into THP1-derived macrophages was measured as described above, with a slight modification of adding a constant concentration of AME antibody to the pseudovirus followed by

varying concentrations of inhibitory antibody. Antibody-pseudovirus mixtures were then incubated for 1 hour before infection and luminescence measurement as described above. Six wells were used for each antibody concentration per biological replicate. To calculate relative entry, background luminescence of spike pseudovirus alone was subtracted from each luminescence value before normalization to the average luminescence for the spike with AME antibody only positive control. Luminescence readings were taken as often as possible over approximately 6 minutes following the addition of luciferin; readings at approximately 0.5, 2.5, and 4.5 minutes were averaged for each well on each day. Media used to culture the THP1 cell line and experiments was RPMI (Gibco) with 10% heat-inactivated FBS (R&D Systems), 100 U/mL Pen-Strep (Gibco), 1 mM sodium pyruvate (Gibco), and 2 mM L-glutamine (Gibco).

These data were fit to a nonlinear regression three-parameter Hill model with a fixed 0 baseline and graphed using GraphPad Prism. These fits were used to calculate AME IC_{50}, defined as the concentration required to reach 50% inhibition of the entry with AME antibody alone, which was calculated for each biological replicate. Further analysis comparing each antibody's AME IC_{50}s to antiN IC_{50} or its respective neutralization IC_{50} were performed using a one-way and two-way ANOVA, respectively, with post hoc Dunnett's test. Additional two-way ANOVAs to compare each antibody's Hill slope to each other antibody's Hill slope and to compare each Hill slope to -1 were performed using post hoc Tukey's and Šidák's tests, respectively. Hill slopes were taken from the nonlinear regression fits described above, and the ANOVAs were also performed using GraphPad Prism.

5.3 Results

5.3.1 Inhibition of AME by Group 2 and Group 5 antibodies

To determine whether individual mAbs are able to inhibit AME and whether antibodies with varying conformational regulation and epitope are differentially effective as AME inhibitors, we tested the Group 1 and Group 4 antibodies for their ability to inhibit entry mediated by the Group 2 and Group 5 antibodies. All the Group 1 and Group 4 antibodies were able to inhibit AME by either the Group 2 or the Group 5 antibody in a concentration-dependent manner **(Figure 6A, 6B)**. Interestingly, Group 4 antibody 2-4 was the most effective inhibitor of Group 2 AME (IC_{50}: 0.059 µg/mL) and the least effective inhibitor of Group 5 AME (IC_{50}: 0.29 µg/mL) **(Figure 6C, 6D)**. This nearly 5-fold lower effectiveness at inhibiting Group 5 vs. Group 2 AME was notably greater in magnitude than the differences in AME IC_{50} for the other 3 inhibitory antibodies, which all differed by under 2-fold. To determine whether the mAbs were inhibiting AME by competitively binding the FcγRs, we also tested the inhibitory ability of an antibody targeting the SARS-CoV-2 nucleocapsid (N), which does not exist in the pseudoviral particles used in this work. This antiN antibody failed to reach 50% inhibition of both Group 2 and Group 5 AME in the equivalent tested concentrations. Additionally, the antiN antibody had a significantly higher IC_{50} for both Group 2 and Group 5 AME than all of the Group 1 and Group 4 inhibitory antibodies **(Figure 6C, 6D)**. These data suggest that both Group 1 and Group 4 antibodies can inhibit AME by both Group 2 antibody DH1047 and Group 5 antibody DH1046, and likely do so through interaction with the SARS-CoV-2 spike protein, rather than exclusively by competing to bind the FcγRs.

After fitting a nonlinear regression Hill model with a fixed 0 baseline to the AME inhibition data, we observed that the Hill coefficients for Group 4 inhibition of Group 2 (mAb DH1047) AME were steeper than those of Group 1 inhibition of Group 2 AME **(Figure 6E)**. The Hill coefficients for the Group 1 antibodies inhibiting Group 2 AME (-1.09 ± 0.15 for CV30 and -1.17 ± 0.18 for C105) were not significantly different from -1, indicating noncooperative binding for both. In contrast, the

Hill coefficients for Group 4 antibodies C144 (-9.00 ± 2.36) and 2-4 (-8.24 ± 6.24) inhibiting Group 2 AME were significantly less than -1 ($p = 0.0003$ and $p = 0.0024$, respectively, for a two-way ANOVA with post hoc Šidák's test), indicating positive cooperativity for both. The Hill coefficient of Group 4 antibody C144 was also significantly lower than those of both Group 1 antibodies. Group 4 antibody 2-4 had a significantly lower Hill coefficient than Group 1 antibody CV30, and had a p-value of 0.0588 when comparing its Hill coefficient to Group 1 antibody C105, nearly reaching statistical significance at the $p \leq 0.05$ level. Overall, these results indicate that while the Group 1 antibodies have no cooperativity when inhibiting Group 2 AME, the Group 4 antibodies have positive cooperativity.

When inhibiting Group 5 (mAb DH1046) AME, the Hill coefficients of the Group 1 antibodies (-1.65 ± 0.21 for CV30 and -1.27 ± 0.44 for C105) did not differ significantly from -1, indicating the same lack of cooperativity shown for Group 2 AME inhibition. When inhibiting Group 5 AME, Group 4 antibody 2-4 similarly had a Hill coefficient that did not significantly differ from -1, indicating lack of cooperativity that contrasts from the positive cooperativity shown for 2-4 when inhibiting Group 2 AME. In contrast, the Hill coefficient of C144 (-13.93 ± 0.96) remained significantly lower than -1 ($p < 0.0001$ for a two- way ANOVA with post hoc Šidák's test), indicating positive cooperativity that was also shown for this antibody when inhibiting Group 2 AME. The Hill coefficient of C144 inhibiting Group 5 AME was also significantly lower than those of the other Group 1 and Group 4 antibodies. Collectively, these results suggest that when inhibiting Group 2 and Group 5 AME, Group 1 antibodies consistently have noncooperative inhibition, but Group 4 antibodies vary, showing both non-cooperativity and positive cooperativity.

We also compared the IC_{50}s for Group 2 and Group 5 AME inhibition of each antibody to its IC_{50} for neutralization of ACE2-mediated entry **(Figure 6F)**. Group 1 antibodies CV30 and C105 and

Group 4 antibody C144 all had AME inhibition IC_{50}s that did not differ significantly from their respective neutralization IC_{50}s. Group 4 antibody 2-4 had a significantly lower AME inhibition IC_{50} than neutralization IC_{50} when inhibiting Group 2 AME, but not when inhibiting Group 5 AME. Relatedly, 2-4 is the only antibody that was more effective (almost 4-fold) at inhibiting Group 2 AME than at neutralizing ACE2-mediated entry when comparing IC_{50}s. Overall, all tested up-exclusive (Group 1) and down-exclusive (Group 4) antibodies were able to inhibit AME by two different antibodies at neutralizing conditions or lower.

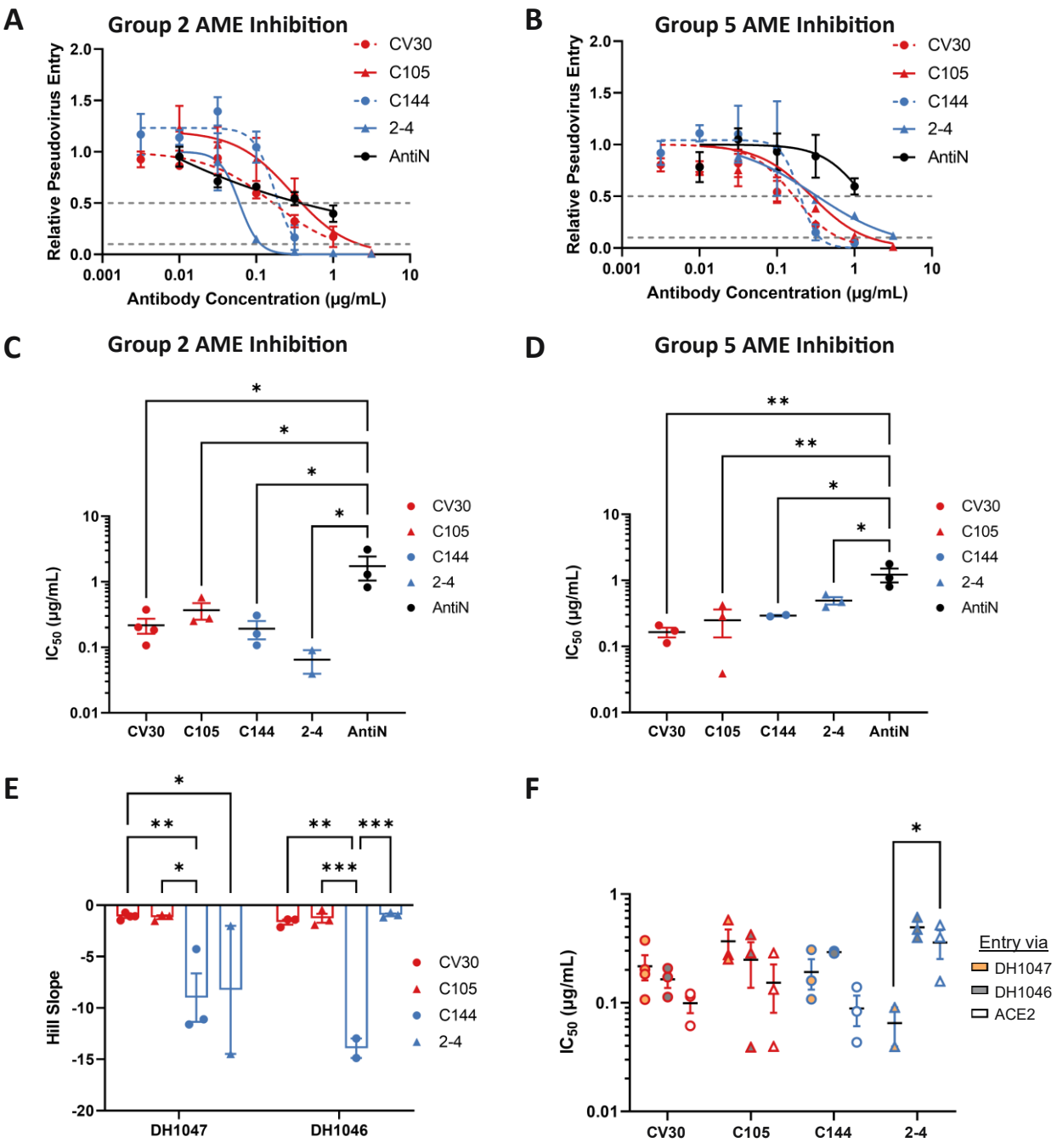
A
Group 2 AME Inhibition
Relative Pseudovirus Entry
Antibody Concentration (µg/mL)
CV30
C105
C144
2-4
AntiN
B
Group 5 AME Inhibition
C
Group 2 AME Inhibition
IC50 (µg/mL)
D
Group 5 AME Inhibition
E
Hill Slope
DH1047
DH1046
F
Entry via
DH1047
DH1046
ACE2

Figure 6. Up-exclusive (Group 1) and down-exclusive (Group 4) antibodies neutralize DH1047-mediated SARS-CoV-2 entry into THP1-derived macrophages.
Entry of SARS-CoV-2-spike-pseudotyped pseudoviral particles in the presence of 1 μg/mL DH1047 (Group 2) or DH1046 (Group 5) and varying concentrations of inhibitory antibodies normalized relative to pseudovirus with DH1047 or DH1046 only. * represents $p \leq 0.05$, ** represents $p \leq 0.01$, and *** represents $p \leq 0.001$. **(A-B)** Grey lines represent 50% (top) and 90% (bottom) inhibition, respectively. Points represent the average ± SEM of 3 biological replicates (for (A), CV30 is 4 replicates, 2-4 is 2 replicates). Lines for each antibody represent nonlinear regression 3 parameter Hill model with a fixed 0 baseline performed in Prism. **(C-D)** IC_{50} for each inhibitory antibody based on nonlinear regression fits shown in (A-B) for each biological replicate; lines represent the average ± SEM of the shown points. p-values shown for ordinary one-way ANOVA with post hoc Dunnett's test. **(E)** Hill slopes from nonlinear fits in (A-B) for each biological replicate; bars represent the average ± SEM of the shown points. p-values shown for two-way ANOVA with post hoc Tukey's test. **(F)** IC_{50}s for neutralization of entry via DH1047 AME, DH1046 AME, and ACE2 for each antibody. Lines and bars represent the average ± SEM for the shown biological replicates. IC_{50}s calculated using nonlinear fits shown in corresponding graphs in Figure 6 and Figure 4. p-values shown for two-way ANOVA with post hoc Dunnett's test.

5.4 Discussion

Given the apparent connection between macrophage and monocyte infection and COVID-19 disease severity[15], investigating the ability of individual mAbs to mediate entry into macrophages *in vitro* is a key step to understanding the effect and clinical relevance of AME on COVID-19 pathology. This work found that both neutralizing mAbs can inhibit AME into macrophages mediated by two different antibodies. Both up-exclusive and down-exclusive antibodies inhibited AME more effectively than a competitor for FcγRs, suggesting that both conformational mechanisms that target the SARS-CoV-2 RBD are more effective at inhibiting AME than antibodies to other targets that compete for FcγRs. This finding supports our hypothesis that conformational and competitive inhibitors of AME differ in their inhibition effectiveness.

The positive cooperativity seen for Group 4 antibodies is likely related to their down-exclusive binding. Group 4 antibodies have been shown to bridge adjacent down RBDs to lock them in the down conformation[5]. This stabilization of multiple down RBDs by a single antibody would likely offer cooperativity for subsequent down-exclusive antibodies to bind and inhibit the up conformation that is required for viral fusion and AME. In particular for Group 2 AME antibody

DH1047, which is known binds largely the inner face exposed only in the up state[1], stabilizing the down state would likely directly impede DH1047 binding and subsequent AME. Structural analysis of the binding of Group 5 AME antibody DH1046 would offer insight into why Group 4 antibody 2-4 loses this cooperative behavior when inhibiting DH1046 AME.

Notably, while Group 1 antibodies overlap in epitope and therefore likely compete with the Group 2 AME antibody, neither Group 4 antibody epitope overlaps at all with that of the Group 2 AME antibody, even when taking into account full epitopes rather than the shared group epitope. This range of antibody overlap in the AME inhibitors suggests that both competitive and noncompetitive spike binders are effective at inhibiting AME. However, additional anti-RBD antibodies that are more conformationally neutral, but do not mediate FcγR-dependent entry, would further explore how conformational or competitive mechanisms differ in their ability to inhibit AME. In addition, expanding the scope of this work to include additional inhibitory antibodies, additional FcγRI AME antibodies, and FcγRIIb AME would allow us to better understand and clarify the role of cooperativity in AME inhibition, other potential differences in effectiveness for up-exclusive and down-exclusive antibodies, and antibody characteristics required to maximize inhibition of AME more broadly.

Further studies using live virus to investigate the effect of this AME on the macrophages would clarify the inflammatory effect of entry mediated by these Group 2 and Group 5 mAbs, and the ability to prevent this inflammatory response by Group 1 and Group 4 mAbs. Preventing the previously demonstrated inflammatory cytokine release and cell death of SARS-CoV-2-infected monocytes and macrophages[15] would offer new approaches to treating COVID-19. Existing SARS-CoV-2 mAb therapeutics have focused on decreasing viral load, but these have shown limited effectiveness when administered to patients who are already hospitalized[58]. Designing

dual-function therapeutics that simultaneously neutralize ACE2 entry to decrease viral load and prevent FcγR-dependent AME to minimize inflammation could offer better therapeutic support for patients at varying stages and severity of disease. Additionally, the identification of epitopes associated with AME vs. AME inhibitory effect could drive future vaccine design to promote development of antibodies that not only avoid AME and any resulting inflammatory response, but also effectively inhibit it.

Chapter VI: Conclusions and Future Directions

Collectively, this work found that anti-SARS-CoV-2 epitope, conformational regulation of the RBD, and AME ability are connected and predictive. We identified unique epitopes for AME antibodies that mediate entry into varying receptors, that also differ from antibodies that do not mediate entry. Understanding this connection could drive the continued development of safe and effective vaccines and therapeutics for COVID-19. For example, our findings suggest that by adding mutations to the specific epitope regions associated with AME, vaccine antigens could be designed to elicit antibodies that simultaneously neutralize ACE2-mediated entry to manage viral load while both avoiding and inhibiting FcγR-dependent entry associated with inflammation.

In addition, we found that antibodies previously shown to mediate entry into FcγRI-expressing cells were able to mediate entry into THP1-derived macrophages and were relatively weakly neutralizing of ACE2-dependent entry. Notably, the AME by these antibodies was inhibitable by neutralizing antibodies with both up-exclusive and down-exclusive binding to the SARS-CoV-2 RBD, which likely inhibit AME by targeting the spike rather than by competing for FcγRs. Overall, these findings suggest that COVID-19 vaccines and therapeutics could be designed to both avoid and inhibit AME without losing neutralization effectiveness, offering a multifaceted approach to improving outcomes for COVID-19 patients. More fundamentally, by finding a correlation between various conformational regulation abilities of antibodies and AME ability, we propose a model for why some, but not all, antibodies mediate FcγR-dependent entry that supports prior work indicating that viral fusion is critical for AME[16].

A primary priority for future work would be to expand the scope of and confidence in our findings with additional antibodies, both that mediate AME and that inhibit it. Better understanding the

fundamental mechanism of AME and AME inhibition is critical to using these findings in applications that benefit patients. In addition, better understanding how effective AME inhibitors are at not only inhibiting AME but also the inflammatory effects of it, which would be possible using the macrophage infection system described here or using monocytes isolated from patient blood, would also support the clinical relevance of this work.

Chapter VII: Project contributions and anticipated publications

7.1 Project contributions and acknowledgements

mAbs DH1041, DH1043, DH1046, and DH1047 were graciously provided by Kevin O. Saunders, Rob Parks, and Alecia Brown (Duke University). mAb CV30 was graciously provided by Neil King and Lauren Carter (University of Washington). mAb 2-4 was graciously provided by David D. Ho, Yang Luo, and Lihong Liu (Columbia University). mAbs C105 and C144, first characterized by Michel C. Nussenzweig (The Rockefeller University), were graciously provided by Pamela J. Bjorkman and Jennifer Keeffe (California Institute of Technology). Pseudoviral plasmids, HEK cell lines, and expertise on pseudoviral experiments were generously provided by Jesse D. Bloom, Katharine H. D. Crawford, and Keara Malone (Fred Hutchinson Cancer Center).THP1 cell line and expertise was graciously provided by Michael Gale, Andrey Shuvarikov, Michael Davis, Elyse Verstelle, and (University of Washington). Consultation on epitope and clash analysis was generously provided by Gianluca Interlandi (University of Washington). Sheamin Kim contributed to the collection of SARS-CoV-2 neutralization, AME, and AME inhibition data.

This project has been supported by the National Institutes of Health (T32EB032787 through the Bioengineering Cardiovascular Training program and 5R01AI119675-05), the National Science Foundation (1824792), the University of Washington Royalty Research Fund (RRF A172852), and the Thomas J. and Barbara D. Cable Endowed Fellowship in Bioengineering.

7.2 Anticipated publications

I am currently preparing a 1st author manuscript on this work on SARS-CoV-2 AME and conformational regulation. I also contributed as 2nd author on a primary research article, summarized in Appendix A, that has been published[59].

References

1. Li, D. *et al.* In vitro and in vivo functions of SARS-CoV-2 infection-enhancing and neutralizing antibodies. *Cell* **184**, 4203–4219 (2021).

2. Ozono, S. *et al.* SARS-CoV-2 D614G spike mutation increases entry efficiency with enhanced ACE2-binding affinity. *Nat Commun* **12**, (2021).

3. Daniloski, Z. *et al.* The spike D614G mutation increases SARS-CoV-2 infection of multiple human cell types. *Elife* **10**, 1–16 (2021).

4. Shang, J. *et al.* Cell entry mechanisms of SARS-CoV-2. *Proc Natl Acad Sci U S A* **117**, (2020).

5. Barnes, C. O. *et al.* SARS-CoV-2 neutralizing antibody structures inform therapeutic strategies. *Nature* **588**, 682–687 (2020).

6. Tortorici, M. A. *et al.* Ultrapotent human antibodies protect against SARS-CoV-2 challenge via multiple mechanisms. *Science (1979)* **370**, 950–957 (2020).

7. Liu, L. *et al.* Potent neutralizing antibodies against multiple epitopes on SARS-CoV-2 spike. *Nature* **584**, 450–456 (2020).

8. Hurlburt, N. K. *et al.* Structural basis for potent neutralization of SARS-CoV-2 and role of antibody affinity maturation. *Nat Commun* **11**, (2020).

9. Benton, D. J. *et al.* Receptor binding and priming of the spike protein of SARS-CoV-2 for membrane fusion. *Nature 2020 588:7837* **588**, 327–330 (2020).

10. Sanyaolu, A. *et al.* SARS-CoV-2 Omicron variant (B.1.1.529): A concern with immune escape. *World J Virol* **11**, 137–143 (2022).

11. Walls, A. C. *et al.* Structure, Function, and Antigenicity of the SARS-CoV-2 Spike Glycoprotein. *Cell* **181**, 281-292.e6 (2020).

12. Jackson, C. B., Farzan, M., Chen, B. & Choe, H. Mechanisms of SARS-CoV-2 entry into cells. *Nat Rev Mol Cell Biol* **23**, 3–20 (2022).

13. Otsuka, R. & Seino, K. Macrophage activation syndrome and COVID-19. *Inflammation and Regneration* **40**, (2020).

14. McGonagle, D., Ramanan, A. v & Bridgewood, C. Immune cartography of macrophage activation syndrome in the COVID-19 era. *Nat Rev Rheumatol* **17**, 145–157 (2021).

15. Junqueira, C. *et al.* FcγR-mediated SARS-CoV-2 infection of monocytes activates inflammation. *Nature* **606**, (2022).

16. Wang, S. *et al.* Antibody-dependent enhancement (ADE) of SARS-CoV-2 pseudoviral infection requires FcγRIIB and virus-antibody complex with bivalent interaction. *Commun Biol* **5**, (2022).

17. Zhou, Y. *et al.* Enhancement versus neutralization by SARS-CoV-2 antibodies from a convalescent donor associates with distinct epitopes on the RBD. *Cell Rep* **34**, 108699 (2021).

18. Wu, N. C. *et al.* An Alternative Binding Mode of IGHV3-53 Antibodies to the SARS-CoV-2 Receptor Binding Domain. *Cell Rep* **33**, (2020).

19. Tang, T. *et al.* Proteolytic Activation of SARS-CoV-2 Spike at the S1/S2 Boundary: Potential Role of Proteases beyond Furin. *ACS Infect Dis* **7**, 264–272 (2021).

20. Bournazos, S., Gupta, A. & Ravetch, J. v. The role of IgG Fc receptors in antibody-dependent enhancement. *Nat Rev Immunol* **20**, (2020).

21. Wu, F. *et al.* Antibody-dependent enhancement (ADE) of SARS-CoV-2 infection in recovered COVID-19 patients: studies based on cellular and structural biology analysis. *medRxiv* 2020.10.08.20209114 (2020).

22. Zheng, J. *et al.* Severe Acute Respiratory Syndrome Coronavirus 2–Induced Immune Activation and Death of Monocyte-Derived Human Macrophages and Dendritic Cells. *J Infect Dis* **223**, 785 (2021).

23. Alzaid, F. *et al.* Monocytopenia, monocyte morphological anomalies and hyperinflammation characterise severe COVID -19 in type 2 diabetes . *EMBO Mol Med* **12**, (2020).

24. Paolini, A. *et al.* Cell death in coronavirus infections: Uncovering its role during COVID-19. *Cells* vol. 10 Preprint at https://doi.org/10.3390/cells10071585 (2021).

25. Farley, C. R. *et al.* FcγRIIB is a T cell checkpoint in antitumor immunity. (2021) doi:10.1172/jci.

26. Bost, P. *et al.* Host-Viral Infection Maps Reveal Signatures of Severe COVID-19 Patients. *Cell* **181**, 1475-1488.e12 (2020).

27. Grant, R. A. *et al.* Circuits between infected macrophages and T cells in SARS-CoV-2 pneumonia. *Nature 2021 590:7847* **590**, 635–641 (2021).

28. Ren, X. *et al.* COVID-19 immune features revealed by a large-scale single-cell transcriptome atlas. *Cell* **184**, 1895 (2021).

29. Song, X. *et al.* Little to no expression of angiotensin-converting enzyme-2 on most human peripheral blood immune cells but highly expressed on tissue macrophages. *Cytometry A* (2020) doi:10.1002/CYTO.A.24285.

30. Baggen, J., Vanstreels, E., Jansen, S. & Daelemans, D. Cellular host factors for SARS-CoV-2 infection. *Nature Microbiology* vol. 6 1219–1232 Preprint at https://doi.org/10.1038/s41564-021-00958-0 (2021).

31. Shen, X.-R. *et al.* Antibody-Dependent Enhancement of SARS-CoV-2 Infection of Human Immune Cells: In Vitro Assessment Provides Insight in COVID-19 Pathogenesis. *Viruses* **13**, (2021).

32. Wieczorek, L. *et al.* Evaluation of Antibody-Dependent Fc-Mediated Viral Entry, as Compared With Neutralization, in SARS-CoV-2 Infection. *Front Immunol* **13**, (2022).

33. Golay, J., Andrea, A. E. & Cattaneo, I. Role of Fc Core Fucosylation in the Effector Function of IgG1 Antibodies. *Frontiers in Immunology* vol. 13 Preprint at https://doi.org/10.3389/fimmu.2022.929895 (2022).

34. Hoepel, W. *et al.* High titers and low fucosylation of early human anti-SARS-CoV-2 IgG promote inflammation by alveolar macrophages. *Sci Transl Med* **13**, 8654 (2021).

35. Chakraborty, S. *et al.* Proinflammatory IgG Fc structures in patients with severe COVID-19. *Nat Immunol* **22**, 67–73 (2021).

36. Chakraborty, S. *et al.* Early non-neutralizing, afucosylated antibody responses are associated with COVID-19 severity. *Sci Transl Med* **14**, 7853 (2022).

37. Maemura, T. *et al.* Antibody-Dependent Enhancement of SARS-CoV-2 Infection Is Mediated by the IgG Receptors FcgRIIA and FcgRIIIA but Does Not Contribute to Aberrant Cytokine Production by Macrophages. *mBio* **12**, (2021).

38. García-Nicolá, O. *et al.* No Evidence for Human Monocyte-Derived Macrophage Infection and Antibody-Mediated Enhancement of SARS-CoV-2 Infection. doi:10.3389/fcimb.2021.644574.

39. Mansbach, R. A. *et al. The SARS-CoV-2 Spike variant D614G favors an open conformational state*. *Sci. Adv* vol. 7 https://www.science.org (2021).

40. Xu, C. *et al.* Conformational dynamics of SARS-CoV-2 trimeric spike glycoprotein in complex with receptor ACE2 revealed by cryo-EM. *Sci Adv* **7**, (2021).

41. Henderson, R. *et al.* Controlling the SARS-CoV-2 spike glycoprotein conformation. *Nat Struct Mol Biol* **27**, 925–933 (2020).

42. Benton, D. J. *et al.* The effect of the D614G substitution on the structure of the spike glycoprotein of SARS-CoV-2. *Proc Natl Acad Sci U S A* **118**, (2021).

43. Korber, B. *et al.* Tracking Changes in SARS-CoV-2 Spike: Evidence that D614G Increases Infectivity of the COVID-19 Virus. *Cell* **182**, 812-827.e19 (2020).

44. Finkelstein, M. T. *et al.* Structural analysis of neutralizing epitopes of the SARS-CoV-2 spike to guide therapy and vaccine design strategies. *Viruses* **13**, (2021).

45. Yuan, M., Liu, H., Wu, N. C. & Wilson, I. A. Recognition of the SARS-CoV-2 receptor binding domain by neutralizing antibodies. *Biochem Biophys Res Commun* **538**, 192 (2021).

46. Barnes, C. O. *et al.* Structures of Human Antibodies Bound to SARS-CoV-2 Spike Reveal Common Epitopes and Recurrent Features of Antibodies. *Cell* **182**, 828-842.e16 (2020).

47. Lan, J. *et al.* Structure of the SARS-CoV-2 spike receptor-binding domain bound to the ACE2 receptor. *Nature* **581**, 215–220 (2020).

48. Zhang, J. *et al.* Structural impact on SARS-CoV-2 spike protein by D614G substitution. *Science (1979)* **372**, 525–530 (2021).

49. Zhan, W. *et al.* Structural Study of SARS-CoV-2 Antibodies Identifies a Broad-Spectrum Antibody That Neutralizes the Omicron Variant by Disassembling the Spike Trimer. *J Virol* **96**, (2022).

50. Yuan, M. *et al.* A highly conserved cryptic epitope in the receptor binding domains of SARS-CoV-2 and SARS-CoV. *Science (1979)* **368**, (2020).

51. Hastie, K. M. *et al.* Defining variant-resistant epitopes targeted by SARS-CoV-2 antibodies: A global consortium study. *Science (1979)* **374**, 478–472 (2021).

52. Greaney, A. J. *et al.* Complete Mapping of Mutations to the SARS-CoV-2 Spike Receptor-Binding Domain that Escape Antibody Recognition. *Cell Host Microbe* **29**, 44-57.e9 (2021).

53. Baxter, E. W. *et al.* Standardized protocols for differentiation of THP-1 cells to macrophages with distinct M(IFNγ+LPS), M(IL-4) and M(IL-10) phenotypes. *J Immunol Methods* **478**, (2020).

54. Nimmerjahn, F. & Ravetch, J. V. Fcγ receptors as regulators of immune responses. *Nat Rev Immunol* **8**, 34–47 (2008).

55. Matveeva, O., Nechipurenko, Y., Lagutkin, D., Yegorov, Y. E. & Kzhyshkowska, J. SARS-CoV-2 infection of phagocytic immune cells and COVID-19 pathology: Antibody-dependent as well as independent cell entry. *Frontiers in Immunology* vol. 13 Preprint at https://doi.org/10.3389/fimmu.2022.1050478 (2022).

56. D Crawford, K. H. *et al.* Protocol and Reagents for Pseudotyping Lentiviral Particles with SARS-CoV-2 Spike Protein for Neutralization Assays. *Viruses* **12**, (2020).

57. Tian, D., Sun, Y., Xu, H. & Ye, Q. The emergence and epidemic characteristics of the highly mutated SARS-CoV-2 Omicron variant. (2022) doi:10.1002/jmv.27643.

58. Taylor, P. C. *et al.* Neutralizing monoclonal antibodies for treatment of COVID-19. *Nat Rev Immunol* **21**, 382–393 (2021).

59. Ludwig, S. G. *et al.* FimH as a scaffold for regulated molecular recognition. *J Biol Eng* **15**, (2021).

Appendix A: FimH as a scaffold for regulated molecular recognition

Excerpts from Ludwig et al. 2021 publication in Journal of Biological Engineering

Project introduction

The ability to trigger binding and release of targets would be highly useful in many areas of biotechnology. Drug delivery, for example, relies on controlling release of the drug payload at the targeted site. Bioseparations takes advantage of capturing and, after flow-through, eluting a desired molecule to isolate or purify it. In diagnostics, sample preparation also benefits from a "capture and release" mechanism for isolating and concentrating desired biomarkers from a sample. In this way, these and many other applications could be improved by the use of regulated recognition proteins.

Several techniques have been shown to create regulated recognition proteins. In drug delivery, cleavable linkers are often added to binding proteins to release the bound drug [1], but this mechanism is irreversible, giving only one-way control upon cleavage. Alternatively, protein domains may be inserted into existing recognition proteins to regulate the activity of the latter [2]. For example, ligand binding at the inserted domain can regulate the parent protein's enzymatic activity [3][4], or capture of its native ligand [5]. A particularly notable example is one where calmodulin, which undergoes a large conformational change upon binding its ligand, is successfully inserted into a variety of single- variable fragments (scFvs) to introduce affinity modulation [6]. This method essentially builds allostery into proteins that were not originally allosteric, but this very advantage also results in large multi-domain proteins. A simpler approach may be to modify the epitope of an already well-studied, allosterically regulated protein, resulting

in a protein scaffold with regulated binding. Scientists often turn to protein scaffolds when generally addressing recognition protein needs, resulting in successful protein scaffolds such as anticalins [7], affibodies [8], affirmers [9], DARPins [10], and over a dozen more [11]. More interesting, however, is the use of scaffolds with innate conformation-dependent binding. This was demonstrated with a repeat-in-toxin domain, whose conformational change to aβ-roll secondary structure upon calcium binding was successfully retained to capture and release the non-native target lysozyme instead [12]. Therefore, it is worth exploring whether other well-characterized, conformationally-regulated proteins can be modified to recognize a new target and retain con-formational regulation of binding. This would provide an additional tool for generating regulated recognition molecules and build upon our fundamental knowledge of the flexibility of conformational regulation.

In this work, we considered the bacterial adhesive protein FimH not only because it undergoes a large con-formational change, resulting in significantly different ligand affinities [13], but also because it is conformationally regulated via more than one mechanism, presenting an interesting challenge for creating conformationally-regulated scaffolds. FimH is the last subunit of long organelles called fimbriae, or pili, protruding from *Escherichia coli* cells, and it consists of two domains connected by a flexible linker. The pilin domain, shown in black in **Figure 7a**, anchors FimH to the rest of the pili via a donated β-strand, while the lectin domain, shown in white in **Figure 7a**, binds to mannose (and, in fact, a wide range of terminal mannosylated compounds, including heptylalpha-D-mannopyrannoside, shown in orange in **Figure 7**).The mannose-binding pocket on the lectin domain contains three exposed loops that interact with mannose; we refer to these as the “CDR” loops to equate them functionally with antibodies’ complementarity-determining regions. These may be ideal sites for mutation recognize alternative ligands. The pilin

domain allosterically regulates binding of mannose via noncovalent interactions with the lectin domain, causing the mannose-binding pocket of FimH to accept a “loose” conformation that has low mannose affinity [13]. These noncovalent interactions may stochastically break, inducing a conformational change in the binding pocket of FimH to tighten around mannose (“tight” conformation), resulting in a highaffinity, long-lived interaction with mannose [13]. In the absence of any trigger, this happens infrequently in wild-type FimH, which strongly prefers the loose conformation. However, certain mutations or triggers can force FimH to switch to the tight conformation. A well-studied example of this trigger is tensile force from fluid drag during bacterial adhesion in flow, resulting in formation of “catch-bond” type interactions between FimH and its ligand that are strengthened by force [17][13].

Triggers other than force can also affect the conformational state of FimH. Some monoclonal antibodies (mab) raised against FimH exhibit conformational specificity. One such antibody, mab21, recognizes FimH and allosterically stabilizes its tight conformation. It does so by binding at a site distal from the CDR loops (shown in green in **Figure 7a**), where it obstructs the noncovalent interactions between the two domains to enable the higher mannose affinity [16][18]. This raises the question of whether mab21 can still allosterically regulate binding of FimH after the CDR loops are mutated to recognize different ligands. Another trigger is mannose itself. Since it stabilizes FimH in the tight conformation, it may also promote this state in mutated FimH if its epitope re-mains intact. This behavior is observed in the presence of the antibody mab926, which binds adjacent to mannose in the binding pocket of FimH, where it stabilizes the loose conformation. Since the epitope of mab926only partially encompasses the binding site of mannose, mab926 and mannose exhibit “parasteric” behavior, a noncompetitive mechanism of inhibition between two ligands with overlapping binding sites [19]. Importantly, soluble mannose,

in the form of methylα-Dmannopyranoside, has been shown to forcibly dissociatemab926 from FimH, which was possible because mannose could bind its epitope and induce the tight state, distorting the mab926 association with FimH. This suggests that mannose could be used as a parasteric trigger for dissociation of other ligands that bind adjacent to mannose in the pocket but preferentially recognize the loose conformation.

FimH has been altered to recognize new targets previously [20][21], but those variants were neither designed nor tested for regulated binding, since the regulation of FimH was not

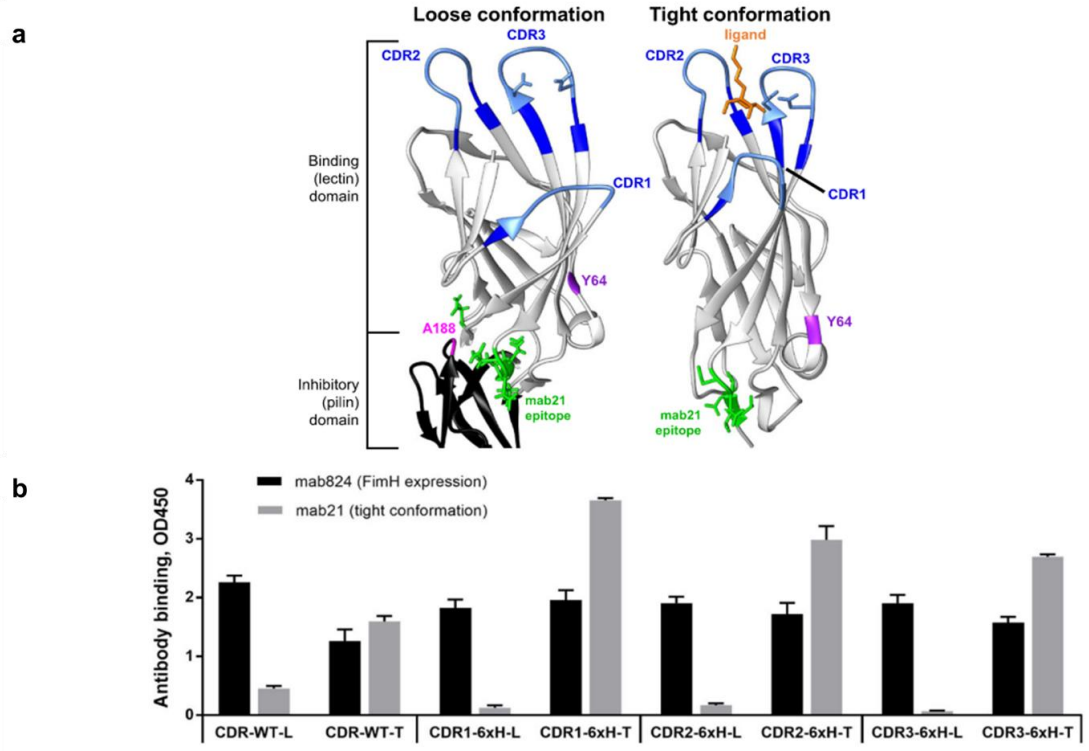

Figure 7. Structure and conformation of FimH lectin domain and the FimH CDR-6xH variants.
(a) The crystal structures of the loose (left, PDB ID: 4XO9, [14]) and tight (right, PDB ID: 1UWF, [15]) conformations of FimH are illustrated. Residues of the CDR loops that are mutated to histidine are in light blue (with those critical for mannose binding, N135 and D140, shown with sticks), and the remaining residues of the CDR loops are in dark blue. The rest of the lectin domain is white, the portion of the pilin domain shown is black, the bound ligand heptyl alpha-D-mannopyrannoside is orange, the residues mutated as “tightening substitutions” are pink (A188) and purple (Y64), and lastly, the epitope of mab21 is green (N29, N152-V156) [16]. **(b)** Binding of pili (CDR-6xH variants or wild-type CDR loops) was tested to mab824 (black bars) for expression and proper folding, and to mab21 (gray bars) to determine expression in the tight conformation. Nonspecific binding was subtracted from all measurements (n= 3, mean ± standard deviation)

understood at the time. We hypothesize that by deliberately mutating only regions of FimH known to contribute to ligand specificity, away from the regulatory region, we can introduce binding to new targets that take advantage of the conformation-dependent regulation of FimH via allosteric and “parasteric” mechanisms.

Here, we show that FimH can serve as a conformationally-regulated scaffold for generating regulated recognition proteins. We demonstrate that all three CDR loops of the FimH pocket are permissive to mutations that can result in recognition of new targets, with-out inhibiting the conformational changes of FimH. While some of these new protein variants may bind their targets with equal affinity in both conformations, we identify several variants that have conformation-dependent binding to their new target using either parasteric or allosteric effectors.

Scaffold design and ELISAs on CDR-6xH variants

To test whether the CDR loops of FimH carry positions that can be varied without destabilizing the protein or preventing conformational changes, a hexa-histidine tag(6xH) was substituted into each loop. This tag was chosen as a model epitope that has been used previously for testing for permissive sites [22]. In the CDR1 loop (10AIPIGGG16), positions I11 to G16 were replaced with six histidine residues, or 6xH. The same was done toD47 to I52 in the CDR2 loop (46NDYPETITD54) or to N135 to D140 in the CDR3 loop (133QTNNYNSDDF142). All mutations were made to the K-12 variant of the *fimH* gene, which we hereafter refer to as CDR-WT-L, because it has wild-type binding loops and prefers the loose conformation in the absence of any regulator [14].These constructs were made in plasmid pBAD-Fim, which has the full structural *fim* operon downstream of the *araBAD* promoter, enabling expression of FimH at the tips of type 1 fimbriae. We refer to the resulting FimH variants as CDR1-6xH-L, CDR2-6xH-L, and CDR3-6xH-L (Table1), where the “-L” reminds us that these variants are expected to prefer the loose

conformation. For expression of pili containing these FimH variants, the plasmids were introduced into *E. coli* MegaX DH10B™cells, a *fim* null strain.

Expression of properly-folded FimH was confirmed by binding of the anti-FimH monoclonal antibody 824 (mab824) to surface-immobilized pili in an ELISA. Mab824 is suitable for this because it recognizes both loose and tight conformations equally (Fig. S1), at a tertiary epitope distal from the CDR loops [19]. As shown in **Figure 7b**, all four "L" FimH variants were not recognized by mab21, confirming that all preferred the loose conformation. Indeed, the introduction of 6xHinto any of the three loops decreased mab21 binding over that observed for CDR-WT-L, suggesting that the bulky histidine residues favor the loose conformation of the pocket.

Therefore, in order to engineer FimH in the tight conformation with these same 6xH-modified loops, additional substitutions, A188D and Y64R, were introduced. We refer to these as "tightening substitutions" because they have been shown to stabilize the tight conformation of the lectin domain [23, 24]. They also lie in regulatory regions far from the CDR loops, as shown in **Figure 7a**. We refer to the resulting variants as CDR-WT-T (wild-type loops with A188D), CDR1-6xH-T (CDR1-6xH withA188D), CDR2-6xH-T (CDR2-6xH with A188D andY64R), and CDR3-6xH-T (CDR3-6xH with A188D andY64R), where the "-T" reminds us that these variants prefer the tight conformation. The addition of A188D was sufficient to enable maximal mab21 binding for FimH with wild-type and CDR1-6xH loops, but FimH with CDR2-6xH and CDR3-6xH additionally required Y64R to induce maximal mab21 binding.

The affinity of the CDR-6xH variants in each conformation for Penta-His was measured in an ELISA by varying the concentration of the antibody and fitting the results with a 1:1 binding model.

For each modified CDR loop, we tested the affinity of the mutant: 1) on its own, 2) upon introducing tightening substitutions, and 3) with tightening substitutions and upon treatment with mab21. The affinity of the CDR1-6xH variants for Penta-His was higher in the tight conformation because the KD decreased 5-fold from 169 ± 16 nM to 38 ± 4 nM with the tightening substitutions, with or without mab21 **(Figure 8a)**. In contrast, the affinity of the CDR2-6xH variants for Penta-His was higher in the loose conformation, because the KD increased by 3-fold, from 7.5 ± 0.4 nM to 21.4 ± 1.1 nM, with the tightening substitutions in CDR2-6xH-T. Addingmab21 to CDR2-6xH-T further increased the KD over 2-fold, to 51 ± 3 nM (for a total of 7-fold increase over CDR2- 6xH-L), demonstrating mab21's potential to act as an effector **(Figure 8b)**. Lastly, the affinity of the CDR3-6xHvariants for Penta-His was similar in both conformations **(Figure 8c)**, because the KD was 2.8 ± 0.3 nM vs. 3.6 ± 0.2nM with and without the tightening substitutions, and adding mab21 did not change the K_D.

BLI on CDR2-6xH

In order to confirm the conformation-dependence of affinity of the CDR-6xH mutants, we measured binding of pili to immobilized Penta-His using Bio-Layer Interferometry (BLI), which offers label-free, real-time kinetics and affinity data. The CDR2-6xH variants were chosen as the test case for this method, to confirm that tightening substitutions led to a difference in affinity. In the shorter timescale of these experiments, the binding of CDR2-6xH-L to Penta-His was relatively complex, in-volving both fast and slow dissociation kinetics. This could not be fit with a 1:1 binding model, but fit a two-state reaction binding model well **(Figure 8d)**. Importantly, wild-type FimH similarly shows two-state binding to mannose, in which the two states differ much more in kinetics than in affinity [25]. In this two-state fit, the measured KD of CDR2-6xH-L to Penta-His was 62.5 ± 33.3 nM (n=3). In contrast, CDR2-6xH-T demonstrated low Penta-His binding **(Figure**

8e), where the level of binding was near the observed noise level for BLI (0.1 nm) [26], even at concentrations 2 to 5 times higher than the K_D of CDR2-6xH-T to Penta-His as measured using ELISA. While it is possible that the low binding level could be quantified with either higher pili concentrations or longer association times, these modifications would make this technique unaffordable, so neither BLI nor other real-time binding techniques were further pursued for affinity data. Nevertheless, because the response after 120 s of association with 100 nM of CDR2-6xH-L pili is significantly higher than that with CDR2-6xH-T pili **(Figure 8f)**, it is clear that the

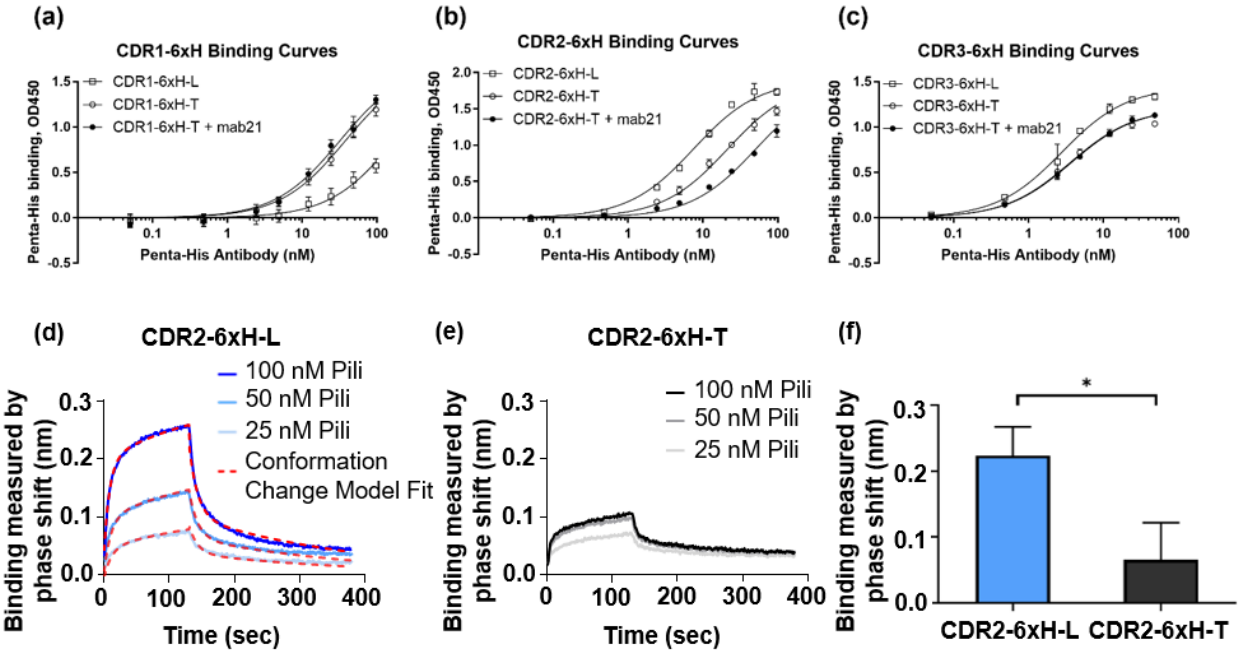

Figure 8. Conformational dependence of binding by CDR-6xH variants to Penta-his antibody.
(a) Binding of Penta-His to CDR1-6xH variants using ELISA, where KD= 169 ± 16 nM (loose conformation, open squares), 38 ± 4 nM (tight conformation, open circles), 32 ± 3 nM (tight conformation + mab21, filled circles). **(b)** Binding of Penta-His to CDR2-6xH variants using ELISA, where KD= 7.5 ± 0.4 nM (loose conformation, open squares), 21 ± 1 nM (tight conformation, open circles), 52 ± 3 nM (tight conformation + mab21, filled circles). **(c)** Binding of Penta-His to CDR3-6xH variants using ELISA, where KD= 2.8 ± 0.3 nM (loose conformation, open squares), 3.6 ± 0.2 nM (tight conformation, open circles), 3.70 ± 0.20 nM (tight conformation + mab21, filled circles). **(d)** Sample data for binding of CDR2-6xH-L pili to Penta-His using bio-layer interferometry (BLI), with a fit to a two-state (conformation change) reaction model. **(e)** Sample data for binding of CDR2-6xH-T pili to Penta-His using BLI showing that binding is not concentration-dependent. **(f)** Binding measured at the end of the association phase during BLI, just before the dissociation phase, for both variants of pili. Binding curves using ELISA (n= 3, mean ± standard deviation) were fitted using GraphPad Prism 7 software using a 1:1 binding model. Error bars in BLI graphs represent the standard deviation of n = 2 experiments on separate days. * indicates $p < 0.05$ by 1-tailed Student's t-test.

CDR2-6xH variants bind better to Penta-His in the loose than in the tight conformation in this assay as well, validating the conformation-dependent binding observed via ELISA.

Selected methods

Strain pBAD-Fim was constructed using *Escherichia coli* cells from the MegaX DH10B™T1RElectrocomp™cell line (Invitrogen™, Carlsbad, CA), a high-transforming derivative of the *fim* null *E. coli* K12 strain [33]. The strain was transformed with the recombinant plasmid pBAD-Fim (10 kb), made from pBAD/HisB (Invitrogen). This contains the full *fim* operon (excluding regulatory subunits *fimB* and *fimE*), inserted into the vector just downstream of its *araBAD* promoter using Gibson Assembly[34]. Point mutations, substitutions, and insertions were introduced to the *fimH* gene in pBAD-Fim using the QuikChange II XL Site-Directed Mutagenesis kit (Agi-lent Technologies, Santa Clara, CA, USA). Primers were designed using the QuikChange Primer Design tool(Agilent Technologies). Mutations were verified by sequencing.

Mouse anti-FimH monoclonal antibodies mab21 andmab824 were described previously [16, 19]. Fab fragments of mab21 were generated using Pierce™Fab Preparation Kit (Thermo Fisher Scientific, Waltham, MA). Fimbriae were purified from the indicated *E. coli* pBAD-Fim strains. Bacteria were grown overnight at 37 °C in LB with 100µg/mL ampicillin, sub-cultured at a 1/100dilution for three hours, and fimbrial expression was induced with 0.2% w/v arabinose overnight. Cells were harvested, and pili purified as described previously [16]. Protein concentration was measured using the Pierce™ BCA protein assay kit (Thermo Fisher Scientific, Waltham, MA) after the pili were heated for 5 min at 99 °Cin 0.1 M HCl.

Microtiter plates were coated with purified pili at 0.1mg/mL in 0.02 M $NaHCO_3$ buffer for 1 h at 37 °C, washed, and blocked for 30 min with 0.2% BSA/PBS. Primary antibody was added in blocking

buffer at concentrations ranging from 0.01µg/mL to 20µg/mL for the anti-6xHis antibody Penta-His (Qiagen, Hilden, Germany), or 5µg/mL for mab824 or mab21. When noted, 2% methylα-D-mannopyranoside or 10µg/mL mab21 fab fragments was added with the primary anti-bodies. After incubation for one hour at 37 °C and 3 washes, HRP-labelled goat anti-mouse IgG Fc secondary antibody (Thermo Fisher Scientific, Waltham, MA) was added at 1:2000 dilution. Following washes, 3,3′,5,5′-tet-ramethylbenzidine, or TMB (KPL, Gaithersburg, MD), was added, the reaction stopped with 0.3 M sulfuric acid, and absorbance measured at 450 nm.

Bio-layer interferometry kinetic assays of purified pili binding directly to Anti-Penta-HIS (HIS1K) Biosensors (ForteBio) was performed in a baseline buffer (BB) of HBS-EP (0.01 M HEPES pH 7.4, 0.15 M NaCl, 3 mM EDTA, 0.005% (v/v) Surfactant P20, pH 7.4) with 0.2%BSA, and 0.1% Tween 20 using an Octet RED96 system (ForteBio). HIS1K sensors were first hydrated in BB for at least 10 min. The sensors were then dipped in BB fora 120-s baseline step before being transferred to wells containing 25–100 nM of purified pili in BB for 125–130 s. After this association step, the sensors were transferred back to the original BB wells for 250–400 s of dis-sociation time. These data were exported using Octet Software and fit to a two-state (conformational change) reaction binding model using BIAevaluation 2.0.4 software (GE Healthcare).

Unless otherwise stated, statistical analyses were performed on GraphPad Prism 7 software (GraphPad, La Jolla, Ca) using either multiple two-tailed t-tests (with corrections for multiple comparisons using the Holm-Šídák method) or two-tailed Welch's t-tests (to correct for unequal variance) comparing each test condition with the control condition. When BLI was used to confirm the difference already observed in ELISA, a one-tailed t-test was used.

Author contribution and notes

I performed the BLI experiments and statistical analysis on CDR2-6xH-L and CDR2-6xH-T **(Figure 8d-f)** and wrote the corresponding section of the paper. Additionally, I edited the full manuscript during the review process. **Figure 7** and **Figure 8** in this excerpt of the paper correspond to Figure 1 and Figure 3, respectively, in the version published in the Journal of Biological Engineering.

Appendix A References

1. Thomas JM, Daugherty PS. Proligands with protease-regulated binding activity identified from cell-displayed prodomain libraries. Protein Sci. 2009;:2053-2059.

2. Ostermeier M. Engineering allosteric protein switches by domain insertion. Protein Engineering, Design, & Selection. 2005;: 359–364.

3. Guntas G, Ostermeier M. Creation of an allosteric enzyme by domain insertion. J Mol Biol. 2004;336(1):263–73.

4. Nicholes N, Date A, Beaujean P, Hawk P, Kanwar M, Ostermeier M. Modular protein switches derived from antibody mimetic proteins. PEDS. 2016;29(2):77–85.

5. Guntas G, Mansell TJ, Kim JR, Ostermeier M. Directed evolution of protein switches and their application to the creation of ligand-binding proteins .Proc Natl Acad Sci U S A. 2005;: 11224–11229.

6. Kellman SJ, Dubel S, Thie H. A strategy to identify linker-based modules for the allosteric regulation of antibody-antigen binding affinities of different scFvs. MAbs. 2017;9(3):404–18.

7. Beste G, Schmidt FS, Stibora T, Skerra A. Small antibody-like proteins with prescribed ligand specificities derived from the lipocalin fold. Proc Natl Acad Sci U S A. 1999;: 1898-1903.

8. Fernandez LA. Prokaryotic expression of antibodies and affibodies. Curr Opin Biotechnol. 2004;15(4):364–73.

9. Stadler LK, Hoffman T, Tomlinson D, Song Q, Lee T, Busby M, et al. Structure–function studies of an engineered scaffold protein derived from Stefin a. II: development and applications of the SQT variant. Protein EngDes Sel. 2011;24:751–63.

10. Skerra A Alternative non-antibody scaffolds for molecular recognition. Curr Opin Biotechnol. 2007;: 295–304.

11. Skrlec K, Strukelj B, Berlec A. Non-immunoglobulin scaffolds: a focus on their targets. Trends Biotechnol. 2015;33(7):408–18.

12. Bulutoglu B, Dooley K, Szilvay G, Blenner M, Banta S. Catch and release: engineered Allosterically regulatedβ-roll peptides enable on/off biomolecular recognition. ACS Synth Biol. 2017;6(9):1732–41.

13. Le Trong I, Aprikian P, Kidd BA, Forero-Shelton M, Tchesnokova V, Rajagopal P, et al. Structural basis for mechanical force regulation of the adhesin FimH via finger trap-like beta sheet twisting. Cell. 2010;141(4):645–55.

14. Sauer MM, Jakob RP, Eras J, Baday S, Eris D, Navarra G, et al. Catch-bond mechanism of the bacterial adhesin FimH. Nat Commun. 2016;: 1–13.

15. Bouckaert J, Berglund J, Schembri M, De Genst E, Cools L, Wuhrer M, et al. Receptor binding studies disclose a novel class of high-affinity inhibitors of the Escherichia Coli Fimh Adhesin. Mol Microbiol. 2005;55(2):441–55.

16. Tchesnokova V, Aprikian P, Yakovenko O, LaRock C, Kidd B, Vogel V, et al. Integrin-like allosteric properties of the catch bond-forming FimH adhesin of Escherichia coli. J Biol Chem. 2008;: 7823–7833.Ludwiget al. Journal of Biological Engineering (2021) 15:3 Page 11 of 12
78

17. Yakovenko O, Sharma S, Forero M, Tchesnokova V, Aprikian P, Kidd B, et al. FimH forms catch bonds that are enhanced by mechanical force due to allosteric regulation. J Biol Chem. 2008;: 11596–11605.

18. Tchesnokova V, Aprikian P, Kisiela D, Gowey S, Korotkova N, Thomas W, et al. Type 1 fimbrial adhesin FimH elicits an immune response that enhances cell adhesion of Escherichia coli. Infect Immun. 2011;79(10):3895–904.

19. Kisiela DI, Avagyan H, Friend D, Jalan A, Gupta SK, Interlandi G, et al. Inhibition and reversal of microbial attachment by an antibody with parasteric activity against the FimH adhesin of uropathogenic E. coli. PLoS Pathog. 2015;: 1–22.

20. Schembri MA, Klemm P. Heterobinary adhesins based on the Escherichia coli FimH fimbrial protein. Appl Environ Microbiol. 1998;64(5):1628–33.

21. Schembri MA, Sokurenko EV, Klemm P. Functional flexibility of the FimH adhesin: insights from a random mutant library. Infect Immun. 2000;68(5):2638–46.

22. Hoffman T, Stadler LKJ, Busby M, Song Q, Buxton AT, Wagner SD, et al. Structure-function studies of an engineered scaffold protein derived from stefin A. I: Development of the SQM variant. Protein Eng Des Sel. 2010;:403–413.

23. Aprikian P, Tchesnokova V, Kidd B, Yakovenko O, Yarov-Yarovoy V, Trinchina E, et al. Interdomain interaction in the FimH adhesin of Escherichia coli regulates the affinity to mannose. J Biol Chem. 2007;: 23437–23446.

24. Rodriguez VB, Kidd BA, Interlandi G, Tchesnokova V, Sokurenko EV, Thomas WE. Allosteric Coupling in the Bacterial Adhesive Protein FimH. J Biol Chem.2013;: 24128–24139.

25. Yakovenko O, Tchesnokova V, Sokurenko EV, Thomas WE. Inactive conformation enhances binding function in physiological conditions. Proceedings of the National Academy of Sciences. 2015;: 9884–9889.

26. Abdiche Y, Malashock D, Pinkerton A, Pons J. Determining kinetics and affinities of protein interactions using a parallel real-time label-free biosensor, the octet. Anal Biochem. 2008;377(2):209–17.

27. Rabbani S, Fiege B, Eris D, Silbermann M, Jakob R, Navarra G, et al. Conformational switch of the bacterial adhesin FimH in the absence of the regulatory domain: engineering a minimalistic allosteric system. J Bio Chem.2018;293(5):1835–49.

28. Gebauer M, Skerra A. Engineering protein scaffolds as next-generation antibody therapeutics. Curr Opin Chem Biol. 2009;: 245–255.

29. Hung CS, Bouckaert J, Hung D, Pinkner J, Widberg C, DeFusco A, et al. Structural basis of tropism of Escherichia coli to the bladder during urinary tract infection. Mol Microbiol. 2002;44(4):903–15.

30. Nilsson LM, Thomas WE, Trintchina E, Vogel V, Sokurenko EV. Catch bond-mediated adhesion without a shear threshold: trimannose versus monomannose interactions with the FimH adhesin of Escherichia coli. J Biol Chem. 2006;281(24):16656–63.

31. Nilsson LM, Thomas WE, Sokurenko E, Vogel V. Beyond induced-fit receptor-ligand interactions: structural changes that can significantly extend bond lifetimes. Structure. 2008;16(7):1047–58.

32. Christopoulos A. Allosteric binding sites on cell-surface receptors: novel targets for drug discovery. Nat Rev Drug Discov. 2002;1(3):198–210.

33. Durfee T, Nelson R, Baldwin S, Plunkett G, Burland V, Mau B, et al. The complete genome sequence of Escherichia coli DH10B: insights into the biology of a laboratory workhorse. J Bacteriol. 2008;190(7):2597–606.

34. Gibson DG, Young L, Chuang RY, Venter JC, Hutchison C, Smith HO. Enzymatic assembly of DNA molecules up to several hundred kilobases. Nat Methods. 2009;: 343–345.